Copyright Warning & Restrictions

The copyright law of the United States (Title 17, United States Code) governs the making of photocopies or other reproductions of copyrighted material.

Under certain conditions specified in the law, libraries and archives are authorized to furnish a photocopy or other reproduction. One of these specified conditions is that the photocopy or reproduction is not to be "used for any purpose other than private study, scholarship, or research." If a, user makes a request for, or later uses, a photocopy or reproduction for purposes in excess of "fair use" that user may be liable for copyright infringement,

This institution reserves the right to refuse to accept a copying order if, in its judgment, fulfillment of the order would involve violation of copyright law.

Please Note: The author retains the copyright while the New Jersey Institute of Technology reserves the right to distribute this thesis or dissertation

Printing note: If you do not wish to print this page, then select "Pages from: first page # to: last page #" on the print dialog screen

ABSTRACT

MEASUREMENT OF STRESSES AND THEIR EFFECT ON TRANSPORT IN THIN FILM BATTERY ELECTRODES

by
Subhajit Rakshit

At the moment, there is a significant push towards environmentally friendly energy production and gasoline-free transportation technologies. As a result, there is a renewed interest in energy storage devices such as lithium-ion batteries which will play a key role in providing energy storage capability for these applications. However, the current battery technology is reaching its limits and may not meet future energy storage demands. The increased demand and the limited lithium reserves in geographically remote areas of the earth will lead to higher cost of Li. The alternative battery technologies, such as sodium-ion batteries, are promising due to their low cost, abundance, and low toxic electrode materials. The electrodes such as silicon (Si), germanium (Ge), tin (Sn), and their alloys have been studied as Li battery anode. These anode materials are known to expand significantly upon reacting with Li and a similar, or more severe, behavior can be expected when they react with Na as the cationic radius of Na is larger than that of Li. Consequently, the anode materials will experience a significant amount of stresses which, if not managed properly, will degrade the electrodes rapidly. The stresses are responsible for cracking, pulverization, and ultimate failure of the electrode, and they also affect the transport phenomena.

A large body of literature exists on electrochemical characterizations of various high capacity lithium and sodium-ion battery electrodes such as Si, Ge, and Sn electrodes. However, real-time chemo-mechanical characterization has not been well

explored much on those battery electrodes because of complicated experimental setup and data acquisition method.

Thin film Ge, Sn, and SiO_2 electrodes are fabricated using various thin film deposition techniques. The fabricated electrodes are electrochemically cycled against Li and Na while recording the variation of electrochemical, mechanical, and transport properties to understand the key factors influencing the performance of the batteries. The real-time stresses during electrochemical cycling are recorded with the help of a multi-beam optical sensor (MOS) setup. A high magnitude of stress is recorded in both Li and Na-ion batteries, which is detrimental to the chemical and mechanical stability of the electrodes. Cycled electrodes are characterized by SEM and AFM to understand the morphological changes of the thin film electrode upon cycling.

The observed mechanics and the electrochemical response of Na-ion battery electrodes are compared to the existing literature on Li-ion battery materials. The data and observations presented in the thesis will be helpful in developing and designing future damage tolerant electrode architecture for future application.

MEASUREMENT OF STRESSES AND THEIR EFFECT ON TRANSPORT IN THIN FILM BATTERY ELECTRODES

by
Subhajit Rakshit

A **Dissertation**
Submitted to the Faculty of
New Jersey Institute of Technology
in Partial Fulfillment of the Requirements for the Degree of
Doctor of Philosophy in Mechanical Engineering

Department of Mechanical and Industrial Engineering

August 2019

APPROVAL PAGE

MEASUREMENT OF STRESSES AND THEIR EFFECT ON TRANSPORT IN THIN FILM BATTERY ELECTRODES

Subhajit Rakshit

Dr. Siva P.V. Nadimpalli, Dissertation Advisor Assoc. Professor of Mechanical and Industrial Engineering, NJIT	Date
Dr. I. Joga Rao, Committee Member Professor/Chair of Mechanical and Industrial Engineering, NJIT	Date
Dr. Pushpendra Singh, Committee Member Professor of Mechanical and Industrial Engineering, NJIT	Date
Dr. Shawn A. Chester, Committee Member Assoc. Professor of Mechanical and Industrial Engineering, NJIT	Date
Dr. Eric Detsi, Committee Member Assist. Prof. of Materials Science and Engineering, UPenn	Date

BIOGRAPHICAL SKETCH

Author: Subhajit Rakshit

Degree: Doctor of Philosophy

Date: August 2019

Undergraduate and Graduate Education:

- Doctor of Philosophy in Mechanical Engineering
  New Jersey Institute of Technology, Newark, NJ, USA, 2019

- Master of Technology in Materials Science and Nanotechnology
  Jadavpur University, Kolkata, India, 2014

- Bachelor of Technology in Electronics and Communication Engineering,
  West Bengal University Technology, Kolkata, India, 2012

Major: Mechanical Engineering

Presentations and Publications:

Rakshit, S., Tripuraneni, R., and Nadimpalli, S.P.V., 2018. Real-time stress measurement in SiO_2 thin films during electrochemical lithiation/delithiation cycling. Experimental Mechanics, 58(4), pp.537-547.

Tripuraneni, R., Rakshit, S., and Nadimpalli, S.P., 2018. In situ measurement of the effect of stress on the chemical diffusion coefficient of Li in high-energy-density electrodes. Journal of The Electrochemical Society, 165(10), pp.A2194-A2202.

Mandal, D., Nunna, B.B., Zhuang, S., Rakshit, S., and Lee, E.S., 2018. Carbon nanotubes based biosensor for detection of cancer antigens (CA-125) under shear flow condition. Nano-Structures & Nano-Objects, 15, pp.180-185.

Rakshit, S., Pakhare, A., Ruiz, O., Khoshi, M.R., He, H., Detsi, E., and Nadimpalli, S.P.V., 2018. Structural changes and associated stress evolution on Ge anode as Na-ion battery electrode during sodiation/desodiation process. (Manuscript under preparation)

Rakshit, S., Welborn, S., Detsi, E., and Nadimpalli, S.P.V., 2018. Effect of porosity on high-energy-density electrode in sodium and lithium-ion battery system. (Manuscript under preparation).

Rakshit, S., Sethuraman, V., and Nadimpalli, S.P.V., 2018. Effect of stress on self-discharging study in high capacity sodium and lithium ion battery anodes. (Manuscript under preparation).

To my family, friends, and teachers.....

ACKNOWLEDGMENT

I would like to extend my sincere gratitude to my adviser, Prof. Siva Nadimpalli, for his continuous guidance, encouragement, and support throughout my research. I am thankful for his valuable suggestions and motivation that helped me to troubleshoot many research problems in the entire journey. He kept faith in me during my early PhD days when I was struggling to make my research samples. We spent a lot of time discussing novel ideas, improving writing skills, designing experiments and talking about different topics. I have been extremely fortunate to have an adviser like him.

I want to thank Prof. I. Joga Rao (NJIT), Prof. Pushpendra Singh (NJIT), Prof. Shawn Chester (NJIT), and Prof. Eric Detsi (University of Pennsylvania) for serving my thesis and dissertation committee and offering helpful suggestions. I would like to extend special thanks to thank Prof. Shawn Chester and Prof. Dibakar Datta for their valuable suggestions, guidance, support and discussion throughout the PhD period.

I am thankful to National Science Foundation (grant no NSFCMMI-1652409) for the funding support during my PhD. I am fortunate to have such wonderful collaborators, Prof. Eric Detsi, Dr. Vijay Sethuraman, and Prof. Huixin He.

I would like to thank all my past and present lab mates in Micro and Nano Mechanics group; Raj, Patrick, Rich, Akshay and Igor. I also want to thank my colleagues in the Mechanical department: Shoulun, Nikola, Bharath, Fangda, Jatin, Abhishek, Suchandra, Vidushi, and Islam for discussing various research topics, practicing presentation and sharing their knowledge. I want to thank to all administrative staff at MIE Departments: Gina, Joe, Aileen, Amber, Greg, and Yvonne for their help in ordering research chemicals/materials supplies and preparing travel reimbursement documents.

I would like to acknowledge Dr. Hiro Yamamoto (University of Pennsylvania), David Jones (University of Pennsylvania), Dr. Roman Akhmechet (Princeton University), and Joseph Palmer (Princeton University) for training me in various micro and nanofabrication tools and techniques. I also want to thank Paul Shao (Princeton University) and John Schreiber (Princeton University) for helping me to get trained in using characterization tools at IAC, Princeton University.

Finally, I would like to express my deepest gratitude to my parents for their endless love and support at every stage of life. This dissertation is a small tribute to my Mom, Dad, and sisters.

TABLE OF CONTENTS

TABLE OF CONTENTS
(Continued)

Chapter **Page**

TABLE OF CONTENTS
(Continued)

Chapter **Page**

LIST OF TABLES

Table **Page**

LIST OF FIGURES

LIST OF FIGURES
(Continued)

LIST OF FIGURES
(Continued)

LIST OF FIGURES
(Continued)

Figure **Page**

CHAPTER 1

INTRODUCTION

1.1 Introduction to Li-ion Battery

Lithium-ion batteries have unparalleled volumetric and gravimetric energy densities among the available battery chemistries which made them the primary choice as energy storage devices in portable electronics.[1-2] Growing environmental concerns have increased the demand for clean energy production and gasoline-free transportation, and lithium-ion batteries will play a key role in addressing these issues. Li-ion batteries have a wide range of application starting from portable electronics devices, electric vehicle, and aviation industries. Figure 1.1 shows a schematic of a Li-ion battery, it has three main components: anode, cathode and electrolyte. During charging/discharging process Li ions travel back and forth between anode and cathode via the electrolyte while electrons travel through external circuit which can be tapped for electrical energy. The materials which form an alloy with Li are used as electrodes and are called intercalation materials, because these materials allow reversible insertion/extraction of Li ions into/from the materials without forming a permanent chemical bond. In general $LiCoO_2$ is used as cathode material in Li-ion battery and graphite is used as anode material. The group IV elements such as Ge, Sn, and Si are being considered as potential candidates as anode materials for future high energy density Li-ion batteries. [2-3]

1.2 Thin Film Battery and Choices of Anode Materials

Generally, the commercial lithium-ion battery anodes are composites (shown in Figure 1.1) made of graphite, conductive additives, and polymer binders. Here, Figure 1.2 shows the schematic of a thin film battery. Thin film electrode configuration is good for characterizing chemcial, electrical, and mechanical properties of battery anodes. [4-8]

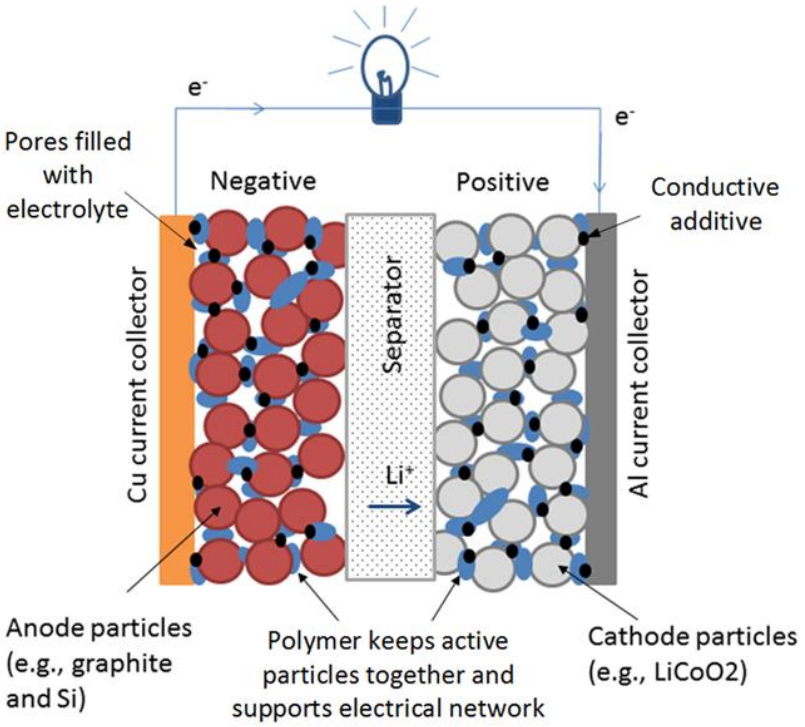

Figure 1.1 Schematic of a commercial Li-ion battery.

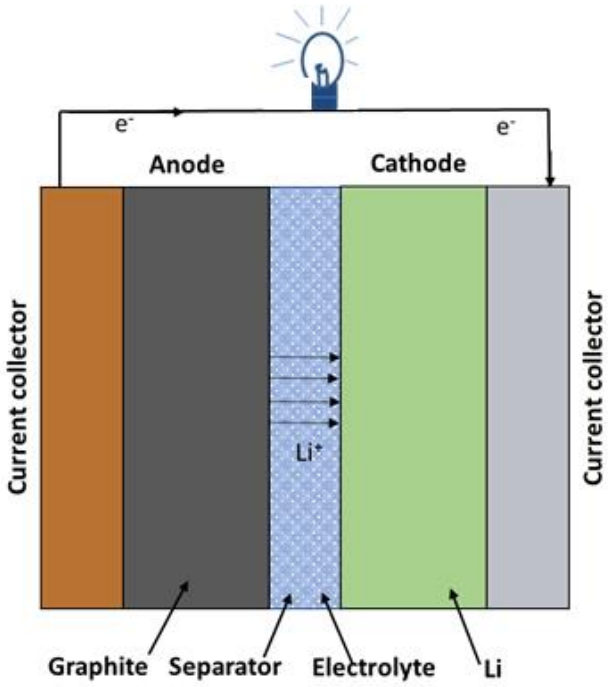

Figure 1.2 Schematic of a thin film Li-ion battery.

1.3 Challenges with Rechargeable Batteries

The next generation material such as Si, Sn, and Ge expand almost 300% upon reacting with Li which induces significant amount of stresses in these electrodes. [9-10] Sethuraman et al., [11-12] Reiner Monig et al.,[13] Nadimpalli et al.,[14] Ostadhossein et al.,[15] Liu et al.,[16] Pharr et al.,[17] and Soni et al., [18]have experimentally showed that the stresses in the Si electrodes could reach as high as 1.5 GPa due to volume changes of electrode materials during battery operation. These volume expansion induced stresses have shown to cause extensive plastic deformation and fracture of electrode particles and rapid capacity fade.[19-21] It was also observed that the mechanical properties such as tensile modulus, Poisson's ratio, and yield stress change with Li concentration which affects this degradation process. For example, Shenoy et al.,[22] showed from first principle

calculations that the elastic modulus values of Si change from 90 GPa at zero lithium concentration to 20 GPa at fully lithiated state (i.e., $Li_{3.75}Si$).

1.4 Beyond Li-ion battery

The increased demand and the limited lithium reserves in politically sensitive and geographically remote areas of the earth will, in future, lead to higher cost of Li. So, alternative rechargeable battery is needed for future application. There are few rechargeable battery technology which attract towards the researcher are mainly Na-ion battery, [23] K-ion battery, [24] Mg-ion battery, [25] and Ca-ion battery. [26] Among them, sodium-ion batteries gained most attention (for energy storage) due to relatively lower cost and abundance of Na. It is expected that a similar volume expansion occurs in materials such as Si, Sn, and Ge upon sodiation/desodiation (i.e., insertion/extraction of sodium into/from the electrode) and their mechanical properties vary with sodium concentration. In fact, the volume expansion due to sodiation could be far greater than that due to lithiation, owing to the fact that Na-ion is larger than Li-ion.[27] Also, Zhu et al.,[28] and Gu et al.,[29] showed from a combined transmission electron microscopy (TEM) and density functional theory (DFT) calculations that the Sn electrodes experience ~ 400 % volume change during sodiation process to form $Na_{15}Sn_4$.[28] This level of volume expansion will lead to stresses that are detrimental to Na-ion electrode and play a crucial role in determining the long term reliability and electrochemical performance of the electrodes. The evolved stresses also affect the transport property inside the battery electrode. Hence, a thorough understanding of the mechanical and electrochemical behavior is required for those anodes before using them as Na-ion battery anodes.

1.5 Focused Work

This work is mainly focused on measuring volume expansion of the anode material, quantifying volume expanion induced stresses, and their affect on transport properties in high-energy-density electrode materials.

1. **Real time stress response of oxide coating in thin film battery during electrochemical charging/discharging**

   Volume expansion induced stress is a major concern for high energy density battery electrodes. Many strtageies to design damage tolerent electrodes such as nanotube, nanowire, nanoporous structures have been proposed. Recent studies show that, oxide coatings improve the cyclic performance of high-energy density electrode materials such as Si to achieve better cyclabity and capacity retention. [30] This oxide coaings are used as clamping layer and provide better chemical and mechanical stability.[16] There are few studies exist on SiO_2 as anode in Li-ion battery and their electrohemical response, however, no study exists on the real-time chemo-mechanical characterization of these oxide coatings.

   Although the material design efforts resulted in innovative core-shell microstructures and the characterization studies helped in understanding electrochemical and structural change behavior of lithiated SiO_2 products, many key questions pertaining to their mechanical behavior remain unanswered. For example, are the reaction products between Li and SiO_2 stronger than lithiated Si? Will the strength of lithiated SiO_2 change during electrochemical cycling? These are all important details which are needed to understand before using them as coating. Also, it is important to understand the Li diffsuivity in a core shell

structure. Diffsuvity is also affected by stress and that will be focused in our next study.

2. Effect of stress on transport properties in Li-ion battery anode

Besides causing mechanical damage, the stresses also affect the reaction kinetics and transport processes which are crucial for a fruitful operation of a battery. [7] Yet, most of the studies which characterize the transport properties of electrodes ignore the effect of stresses on the transport phenomenon. As a result, the measured diffusivity values of Li in a given electrode under similar electrochemical conditions varied significantly (i.e., orders of magnitude difference) among different studies; for example, Ding et al., [7] and Ruffo et al., [31] observed experimentally that the diffusion coefficient in silicon anode values range between 10^{-16} to 10^{-10} cm^2 /sec, which is several orders of magnitude difference. [32] The stress plays a crucial rolein Li transport, hence, it needs to be investigated. Quantitative information about the transport phenomenon is essential to understand diffusion mechanisms and designing effective electrode architectures to optimize the power density and energy density of electrode materials. For example, mathematical models which attempt to simulate a range of physics from only electrochemistry to coupled electrochemistry and mechanics, rely on Li-ion diffusivities in active materials to predict key electrode characteristics such as charge/discharge rates, open circuit potentials, intercalation kinetics, and electrode stresses. Hence, reliable and accurate transport properties are critical for these models to accurately simulate battery operations either at a particle level or at an

overall battery level for effective optimization of electrode microstructures. A precise method of diffusion coefficient measurement not only provides these properties but is also necessary to characterize the transport behavior of emerging electrode materials. In previous studies it has shown that stress affect the transport properties. The standard techniques GITT and PITT were used extensively to measure the Li diffsuivity. However no such studies exist that eplained the effect of stress on diffusivity. [33-34] Here, Ge thin film was choosen as Li-ion battery anode to perform this study.

3. Structural changes and associated stress response of Ge thin film as Na-ion battery anode

Among alternative battery technology, Na ion battery is gaining worldwide attention due its lower cost and similar electrochemistry like Li. [23][35] The cationic radii of Na is more than Li which could generate more stress. It is very interesting to understand the effect of ion size in evolved stress as well as in kinetics and transport properties. There are few studies exist on the chemo-mechanical characterization of Li-ion battery anodes, however no such studies exist on Na-ion battery anode. Not only measuring stress, it is also important to measure the volume expansion of the anode material at different Na-ion concentration which will define the thorough stress in a battery anode. In this study, Ge thin film was incorporated as Na-ion battery anode.

Realizing the important role played by the mechanics phenomenon in battery operation, especially in batteries with large volume expansion electrode materials, a

significant number of research groups have been developing theoretical models for batteries incorporating relevant phenomenon, i.e., electrochemistry, diffusion in solids, large deformation kinematics, and elastic-viscoplastic material behavior.[12][36-38] These experimental studies and models are essential for rapid advancement of battery technology, because they can be valuable in guiding the design of electrode microstructures that are defect tolerant and reliable for thousands of cycles. This is an important factor for the batteries to be considered viable for electric car applications. Although the chemo-mechamical behaviour of various Li-ion battery electrodes, by treating a range of phenomena such as crystalline to amorphous phase transformations, is rapidly progressing; the efforts on Na-ion battery side is almost nonexistent partly due to the lack of experimental data on the mechanical behavior of Na-ion battery electrodes. Hence, this gap in literature is what this PhD is aiming to address.

1.5 Objectives

The main objectives of this thesis are:

- In situ measurement of flow stress and mechanical property variation as a function of Li concentration in oxide thin film as Li-ion battery during charge/discharging cycling
- Measurement of the effect of stresses on the transport phenomenon, i.e., effect of stress on Li-ion diffusivity in Ge electrode under various electrochemical and mechanical loading conditions

- Measure the effect of ion size on the stress evolution in Ge electrode during electrochemical cycling and to compare the performance of Ge thin film as Li as well as Na-ion battery anode

1.6 Outline of this Desertation

Chapter 1 describes the oxide lithiation/delithiation and associated stress measurement on SiO_2 thin film electrode as Li-ion battery anode. This chapter explains the chemo-mechanical characterization of SiO_2 thin film anode and its morphological changes after cycling.

Chapter 2 presents the effect of stress on Li transport phenomena. This chapter shows the Li diffsuivity and associated stress measurement on thin film Ge anode by GITT and PITT methods.

Chapter 3 describes the transition of rechargeable batteries from Li-ion to Na-ion. Also explain the stress evolution on Ge thin film as Na-ion battery during charging/discharging time.

CHAPTER 2

REAL-TIME STRESS MEASUREMENT IN SiO_2 THIN FILMS DURING ELECTROCHEMICAL LITHIATION/DELITHIATION CYCLING

2.1 Introduction

Lithium-ion batteries played a key role in the success of portable electronics. Requirements for clean energy production and low carbon emissions from environmental concerns are driving the advancement of electric vehicle and non-conventional energy production technologies, and lithium-ion batteries are going to play a crucial role in the success of these technologies as well. The energy density and capacity of current lithium-ion batteries, which is limited by their electrode materials, are not adequate to meet the future energy demands. Higher capacities can be achieved [39] by replacing the existing electrode materials with high energy density materials. For example, by replacing graphite (anode in the current lithium-ion batteries) with Si, an immediate improvement of 30% on the overall battery capacity can be achieved which is a significant improvement. However, Si and other high energy density anode materials such as Sn and Al suffer from poor cyclic performance due to volume expansion-induced stresses and associated electrode fracture. [20-21][40] Fracture of electrode particles not only leads to mechanical degradation but also contributes to chemical degradation, because of the formation of solid electrolyte interphase (SEI) layer on fresh fracture surfaces, causing additional capacity loss. [41-44]

The SEI layer or passivation layer forms on anode surfaces during charging and discharging cycles due to the decomposition of electrolyte. [41-43] While this layer imparts kinetic stability to the electrolyte against further reaction in subsequent cycles, it leads to an irreversible loss of Li and battery capacity.[45-47] Most of the capacity loss observed

in the first lithiation/delithiation cycle of secondary lithium-ion batteries is due to this SEI layer formation. In general, the SEI layer formation is a self-limiting reaction, i.e., the reaction (or SEI formation) rate decreases significantly after the SEI layer reaches a critical thickness. However, the large volume changes of Si (or other active) particles during lithiation/ delithiation cycles deform or stretch the SEI layer to a critical level and cause the layer to fail. The continuous failure and reformation of the SEI layer during lithiation/delithiation cycles not only causes capacity loss but also leads to an increase in the resistance to Li-ion diffusion (i.e., internal impedance of a battery). [48] Hence, a chemically and mechanically stable SEI layer is another key factor for improving the cyclic performance of high energy density batteries. [41-43]

Recent studies [9][49-51] have shown that surface coatings such as SiO_2 on nanoparticles and nanotubes can improve the cyclic performance of high energy density electrode materials by minimizing the mechanical degradation and also stabilizing the SEI layers. It has been hypothesized that the coatings impart chemical stability by isolating the active surfaces from the electrolyte and mechanical stability by preventing volume expansion of the active particle beyond a critical level by constraining or clamping it. [49] It has been argued that the clamping action of SiO_2 potentially minimizes the expansion of Si particles, which reduces the deformation and stress levels in SEI and provides mechanical stability to the SEI layer.

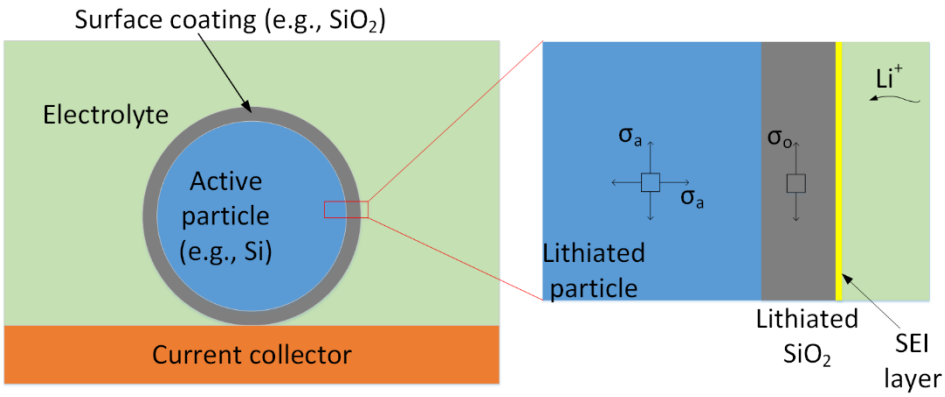

Figure 2.1 Schematic of an active particle (Si) with oxide coating. The zoomed view shows that volume expansion of Si due to lithiation induces stresses in the, Si particle, SiO_2 coating, and SEI. Also, the oxide layer isolates the active particle from the electrolyte producing a stable SEI layer.

Consequently, SiO_2 coatings on Si with different electrode configurations i.e., core-shell type nanoparticles and nanotubes with solid and hollow core (e.g., see Figure 2.1), have been investigated as potential electrode microstructures; SiO_2 coatings on Si [49-50][52] and a SiOC [53] coating on Si are some examples. Although SiO_2 was assumed to be inert to lithium, Sun et al. [54] showed that it reacted with Li reversibly resulting in stable capacities of 500 mAh/g for hundreds of cycles. XRD measurements by Chang et al. [30] showed that crystalline SiO_2 is indeed inert and does not react with Li, but amorphous SiO_2 reacts with it due to the valance charge differences in crystalline and amorphous configurations. As a result, in addition to use as a coating material, SiO_2 is also being considered as a potential anode material due to its higher theoretical capacity compared to conventional carbon-based anode materials. [30][54-58]

The capacity of SiO_2 depends on the reaction products between SiO_2 and Li. Amorphous SiO_2 reacts with Li in a two-step reaction process with the following (Equations (2.1–2.6)) possible mechanisms, [58]

$$5SiO_2 + 4Li^+ + 4e^- \leftrightarrow 2Li_2Si_2O_5 + Si \quad (2.1)$$
$$5Si + 22Li^+ + 22e^- \leftrightarrow Li_{22}Si_5 \quad (2.2)$$

$$2SiO_2 + 4Li^+ + 4e^- \rightarrow Li_4SiO_4 + Si \quad (2.3)$$
$$5Si + 22Li^+ + 22e^- \leftrightarrow Li_{22}Si_5 \quad (2.4)$$

$$SiO_2 + 4Li^+ + 4e^- \rightarrow 2Li_2O + Si \quad (2.5)$$
$$5Si + 22Li^+ + 22e^- \leftrightarrow Li_{22}Si_5 \quad (2.6)$$

Lithium metal initially reacts with SiO_2 to produce lithium silicates ($Li_2Si_2O_5$ and Li_4SiO_4), lithium oxide (Li_2O), and Si; the Si produced in the first step then reacts with Li to produce lithiated Si. According to Yan et al., [58] reaction 1 (Equations (2.1) and (2.2)) alone results in a theoretical reversible capacity of 749 mAh/g, reaction 2 (Equations (2.3) and (2.4)) alone results in 980 mAh/g, and reaction 3 (i.e., Equations (2.5) and (2.6)) alone results in 1961 mAh/g. Depending on the sample configuration (nanoparticle, nanotube, or thin film); electrochemical conditions (charge rates, potentials, or potential sweep rate); and type of materials in contact (electrolyte and constituents of composite electrode), either one reaction, a combination of two concurrent reactions, or all possible reaction mechanisms occur simultaneously in SiO_2 samples during lithiation/delithiation. Further, (Equations (2.1-2.2)) shows reversible reaction, and (Equations (2.3-2.4) and (2.5-2.6)) show irreversible reactions. For example, Sun et al. [54] cycled thin-film SiO_2 and found $Li_2Si_2O_5$ and LixSi phases in their sample at the end of lithiation. They were able to cycle the films reversibly with stable capacities of ~500 mAh/g, suggesting that the $Li_2Si_2O_5$ reaction is reversible; this was also confirmed by several other studies. [30][49][58] Conversely, Zhang et al., [52] Favors et al., [56] Phillippe et al., [59] and Guo et al., [57] observed that their samples only contained Li_4SiO_4 and Li_2O products with LixSi phase undetectable in some cases, and found that these two reactions are irreversible; hence, the lithium consumed to form these products is not recoverable after formation. Yan et al. [58]

cycled hollow porous SiO_2 nanocubes and observed all three products ($Li_2Si_2O_5$, Li_4SiO_4, and Li_2O) in their sample. Therefore, the capacity of the SiO_2 anode depends on the number and type of (Equations (2.1-2.6) reactions taking place in the sample. Nevertheless, some or all of these possible reactions lead to significantly higher capacities compared to the capacity of graphite which is 372 mAh/g.

Although the material design efforts [9][49-51] resulted in innovative core-shell microstructures and the characterization studies [30][54-58] helped in understanding electrochemical and structural change behavior of lithiated SiO_2 products, many key questions pertaining to their mechanical behavior remain unanswered. For example, are the reaction products between Li and SiO_2 stronger than lithiated Si? Will the strength of lithiated SiO_2 change during electrochemical cycling? What level of stresses are generated in the SiO_2 coating during electrochemical cycling? Also, the above studies on coated electrodes provide qualitative understanding only and do not provide quantitative understanding. Several studies [11][13-14][60-62] reported that the mechanical properties of electrode materials (both anodes and cathodes) change during electrochemical cycling; and similarly, the properties of SiO_2 may change continuously during the lithiation/delithiation process due to the formation and decomposition of reaction products in (Equations (2.1-2.6). This knowledge is necessary to develop durable Si/SiO_2 core shell structures or just SiO_2-based electrodes. For example, note, from Figure 2.1, that the oxide layer (or shell) should be able to sustain the deformation and stress levels imposed by the volume expansion of active (core) materials (which could be 300% for Si) to be successful in promoting SEI stability and mechanical integrity for the long cyclic-life operation of the oxide-coated battery electrodes. Despite the importance, no experimental study exists on

the mechanical properties or stress measurement of the lithiated silicon dioxide. Due to the lack of experimental data on the mechanical properties of lithiated SiO_2, existing studies model the coating as simple linear elastic or elastic-plastic material with estimated properties.

Hence, the primary objective of this study is to measure the magnitude of stresses generated in SiO_2 material, understand how these stresses vary during electrochemical cycling, and further, understand how the variation of mechanical properties affect the mechanics of core-shell type of particles. To this end, real-time stress evolution in SiO_2 thin films was measured during lithiation/delithiation cycling using substrate curvature method. A simple finite element model of a Si nanotube coated with a thin layer of SiO_2 was developed using the material properties measured from the experiments. The hollow nanotube developed in the FE model was then lithiated/ delithiated to see how the stresses would evolve in the particles when experimentally measured mechanical properties of lithiated oxide layer were used as opposed to a simple elasticplastic assumption. This study provides basic mechanical properties and an understanding of mechanics that will help in the design of high-energy-density and durable SiO_2-based electrode microstructures.

2.2 Experimental Methods

2.2.1 Electrode Fabrication and Electrochemical Cell Assembly Electrode Fabrication and Electrochemical Cell Assembly Electrode samples were prepared by depositing thin films of Ti (~5 nm, as adhesive layer), Fe (~200 nm, as current collector), and a 100 nm amorphous SiO_2 (or a-SiO_2) on a double side polished fused silica substrate ((50.8 mm diameter and ~500 μm thickness); (Figure 2.2a)) inset shows the details of the films. The

Ti and Fe films were deposited using DC sputtering whereas SiO_2 film was deposited using RF sputtering technique. The deposition rate of SiO_2 film was 1 nm per minute. Process pressure during the deposition of all these films was maintained at 3 mTorr. The substrate platen on which the samples were mounted was rotated at 20 RPM during the deposition process to minimize the variation of film thickness. The planar thin film geometry used in this study eliminates the effect of binders and other additives of a composite electrode, and it allows for an accurate characterization of mechanical and electrochemical behavior of SiO_2. Hence, the thin film on substrate samples is ideal to study the fundamental mechanical behavior of electrodes.

A homemade electrochemical beaker cell was assembled in an argon filled glovebox (MBraun Inc., maintained at 25 °C with less than 0.1 ppm of O_2 and H_2O) by using the deposited SiO_2 film on elastic substrate (sample details can be seen in the ((Figure 2.2a) inset) as a working electrode and a 1.5 mm thin lithium foil as a counter/reference electrode. A polymer separator (Celgard Inc.) was used to prevent physical contact between electrodes, and a 1 M $LiPF_6$ in a 1:1:1 ratio (wt%) of ethylene carbonate (EC): diethyl carbonate (DEC): dimethyl carbonate (DMC) was used as the electrolyte. The casing of the cell was made from Teflon, the cap of the cell was made from stainless steel; the cap has a glass window which enables optical access to the sample for substrate curvature measurements using laser setup show in (Figure 2.2).

2.2.1 Electrochemical Measurements The amorphous SiO_2 films were lithiated and de-lithiated under a galvanostatic, i.e., constant, current density of $i \sim 2\ \mu A/cm^2$, conditions between 3 V and 0.01 V vs. Li/Li+ using Solartron 1470 E potentiostat; the stress and potential response of the sample were recorded during this process. This current density

was chosen to avoid any concentration (or stress) gradients within the SiO_2 thin film during electrochemical cycling. Some cells were interrupted after the first lithiation process and after the subsequent delithiation process; a portion of the electrode sample was separated each time while the remaining portion of the electrode was cycled further. The harvested samples were then soaked for 5 min and rinsed in dimethyl carbonate, then transported in to the SEM chamber for analysis. Care was taken to minimize the exposure of samples to ambient atmosphere during the transfer. This SEM analysis was carried out to ascertain if the SiO_2 films developed any cracks and if so, when they occurred.

2.2.2 Stress Measurement Using MOS Setup Stress evolution in an a-SiO_2 electrode during lithiation/ delithiation cycling was measured by monitoring the changes in the curvature of fused silica substrate with the help of a multi-beam optical sensor (MOS) setup (k-Space Associates, Dexter, MI), illustrated in (Figure 2.2a). The MOS setup has a laser source which produces a single collimated beam and two etalons that were arranged to generate a 2 × 2 array of laser beams. The array of beams reflected from the sample surface (Figure 2.2a) is captured by a CCD camera, and appears as a 2×2 array of circular dots (cross section of the laser beams) on a computer monitor. The sample curvature could be determined by measuring the relative displacement of the center of these laser spots as,

$$\kappa = \frac{\cos \emptyset}{2L}\left\{\frac{D-D_o}{D_o}\right\} \tag{2.7}$$

where D is the distance between the center of laser spots, Do is the initial distance, ; is the angle of the laser beam as defined in (Figure 2.2b), and L is the optical path length as shown in (Figure 2.2b). The factor cos φ/2L is known as the mirror constant, which is specific to a given setup; hence, it is obtained by calibrating the system with a mirror of known

curvature. The 2×2 array of the laser spots enables curvature measurement in two orthogonal directions. Note, from (Figure 2.2a), that although the Li foil, separator, and SiO_2 films were submerged in the electrolyte, the surface of the elastic substrate from which the laser beams were reflected was not submerged. This was done to prevent the complexities associated with the laser beams going through the electrolyte.

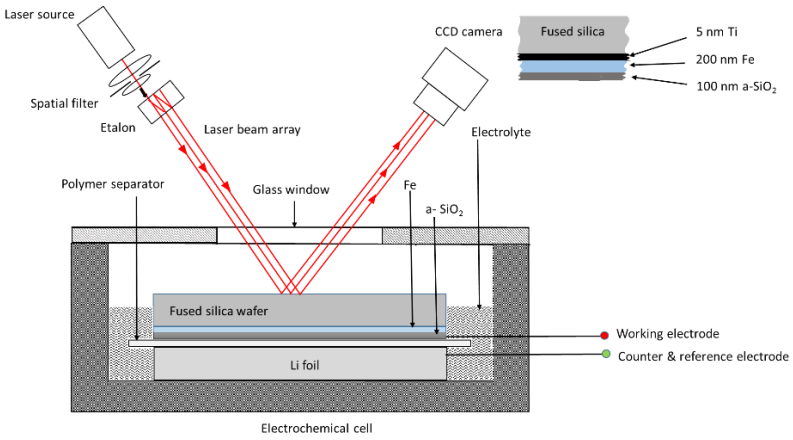

(a)

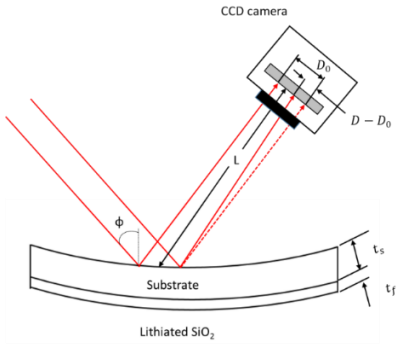

(b)

Figure 2.2 Electrochemical cell with MOS set up for stress measurement is shown in (a) and various relevant optical parameters are defined in (b)

The biaxial stresses in the SiO_2 film are related to the substrate curvature by Stoney's equation

$$\sigma = \frac{E_s t_s^2 k}{6 t_f (1-\upsilon_s)} \tag{2.8}$$

Where Es is Young's modulus of the substrate and ts is the thickness of the substrate, υ_s is Poisson's ratio of substrate, and t_f is the thickness of the SiO_2 film. The film thickness t_f in (Equation (2.8)) will evolve continuously during the experiment due to the chemical reaction between SiO_2 and Li. Although there are no direct, well-controlled experiments on thickness evolution measurements of lithiated SiO_2, first-order estimates can be made. It was observed from a TEM analysis that lithiation of SiO_2 may result in a volumetric strain of 230%; [52] similarly, Li reaction with SiO results in a volume expansion of 200%. [55] Further, Zhang et al. [52] showed, from DFT and MD calculations, that the volume (or film thickness in the current samples) of lithiated SiO_2 increases linearly with the state of charge. Hence, though the volume expansion depends on the type of reactions that are occurring in the film, it is reasonable to assume that SiO_2 expands linearly during lithiation as per (equation (2.9)),

$$t_f = t_f^0 (1 + 2z) \tag{2.9}$$

Here t_f^0 is initial film thickness and z is state of charge (SOC) which changes between 0 and 1; z =1 indicates a capacity of 749 mAh/g and a volumetric strain of 2.

2.2.4 Finite Element Model Figure 2.3a shows the schematic of an amorphous silicon nanotube (internal and external radii of 140 nm and 160 nm, respectively) with a uniform SiO_2 coating of 10 nm thickness considered for simulation; although these dimensions were

selected based on typical Si/SiO_2 nanotube dimensions published in the literature [49], the model is more general and the observations are applicable to other particle dimensions. The finite element package Abaqus was used to simulate the lithiation/delithiation process of the Si nanotube coated with SiO_2. Three different simulations were carried out: 1) a bare Si nanotube was lithiated and delithiated without SiO_2 coating to get the baseline behavior, 2) SiO_2 coating was treated as an elastic-plastic mechanical constraint layer (with $\sigma y = 2.52$ GPa [49]) that allows lithium-ions to pass through but doesn't react or undergo volume expansion a SiO_2 coating was treated as elastic-perfectly plastic material where concentration-dependent yield stress was obtained from the in-situ stress experiments.

Figure 2.3b shows the finite element mesh of the Si nanotube coated with SiO_2, which contains 7380 linear plain strain elements and 7656 nodes, with appropriate boundary conditions. The interface between Si and SiO_2 is assumed to be perfectly bonded. To maintain focus on the mechanics, the solid electrolyte interface formation on the electrode particle was ignored, and a simple model for Li diffusion was adopted where stress coupling is ignored.

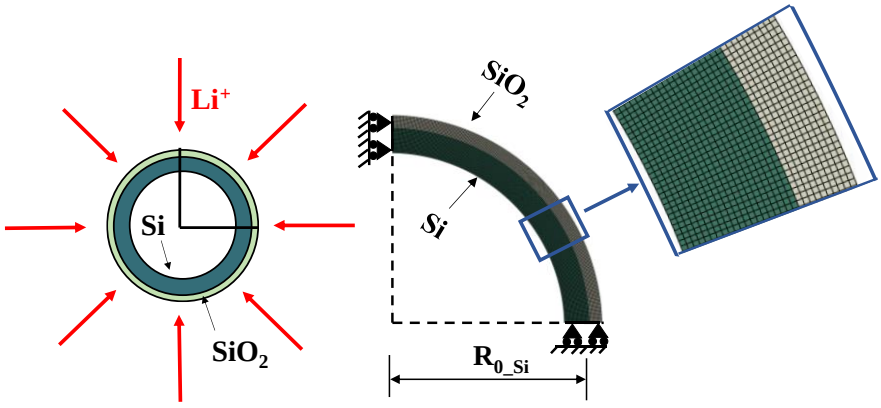

Figure 2.3 Schematic of Si nanotube coated with SiO_2 is shows in (a) and the plane strain finite element mesh (quarter of model due to symmetry) along with symmetry boundary conditions are shown in (b)

2.3 Results and Discussion

2.3.1 Electrochemical and Mechanical Behavior of SiO_2 Film during Charging/Discharging Cycling Figure 2.4a shows SiO_2 electrode potential as a function of electrode capacity during electrochemical cycling under galvanostatic conditions (i.e., constant i = 2 μA/cm^2 corresponding to C/9 rate). The open circuit potential of pristine (or as prepared) SiO_2 film was about 3.0 V vs. Li/Li$^+$, and upon lithiation it drops rapidly to approximately 1.6 V vs. Li/Li$^+$ where a small pseudo plateau was observed. This plateau was nonexistent in the remaining cycles and occurred at a potential higher than the electrolyte decomposition potentials; hence, this could be attributed to an irreversible reaction between SiO_2 and Li which was also reported in earlier studies. [58-63] With further lithiation, the potential rapidly drops again from 1.6 to 1.0 V vs. Li/Li$^+$ and thereafter decreases gradually (almost linearly) to 0.6 V vs. Li/Li$^+$ at 600 mAh/g. As the potential in this linearly decreasing region is higher than the lithiation potential of Si (which is below 0.4 V vs. Li/Li$^+$), most of the lithiation in this region probably leads to the formation of lithium silicates, lithium oxides, and Si: i.e., only the first step in the reactions showed in Equations (2.1- 2.6). Beyond 0.6 V vs. Li/Li$^+$ the potential decreases rapidly to 0.01 V vs. Li/Li$^+$, leading to a total first-cycle lithiation capacity of 760 mAh/g. The second reaction step between Li and pure Si shown in Equations (2.1- 2.6) occurs at potentials below 0.4 V vs. Li/Li$^+$; note from Figure 2.4a that the capacity corresponding to these reactions (where Si could have reacted with Li) is merely ~100 mAh/g. Hence, it can be assumed that the amount of Si produced during the lithiation of SiO_2 thin films and the associated volume changes may be negligible compared to the contribution from the other products in Equations (2.1- 2.6). Upon delithiation, the potential increases quickly to 1.2 V vs. Li/Li$^+$

within a capacity change of 120 mAh/g, followed by a gradual increase until 2.0 V vs. Li/Li^+ is reached at 240 mAh/g, and a sharp rise to 3 V vs. Li/Li^+ thereafter.

The potential response of the SiO_2 film during the first lithiation process is significantly different from that of subsequent lithiation cycles. This could be due to a combination of factors, such as SEI formation, and irreversible chemical reactions (Equations (2.1) and (2.3)) that mainly occur in the first cycle. In other words, the film in the second cycle is not the same as the pristine SiO_2 film and contains some irreversible reactions products, such as Li_4SiO_4 and Li_2O; this is reflected in the differences in the electrode potentials of first and second lithiation processes. Due to the irreversible reactions, such as the formation of lithium silicates, Li_2O, SEI, and possible entrapment of Li, there will be some capacity loss during the cycling process, and it will be severe in the first cycle. For example, note from Figure 2.4b that the first cycle lithiation capacity of SiO_2 film is 760 mAh/g and the delithiation capacity is 600 mAh/g: i.e., a loss of about 160 mAh/g at a coulombic efficiency of 78%. The coulombic efficiency quickly increases to 99% (i.e., negligible loss) from the second cycle with a stable delithiation capacity of 600 mAh/g as shown in Figure 2.4b. It can be assumed that this 600 mAh/g of reversible capacity is mainly due to the reversible reaction shown in Equation (2.1) (i.e., formation/decomposition of Li_2SiO_5) and not due to formation of lithiated Si. This is because the potentials at which these reactions are occurring are clearly above 0.4 V *vs.* Li/Li^+, where Li may not react with Si (hence cannot contribute to the capacity).

Unlike the crystalline Si, volume expansion of lithiated SiO_2 seems to be uniform and isotropic. Figure 2.5a shows that the substrate curvature (which is proportional to stress times film thickness according to Equation (2.8) as a function of time during

electrochemical cycling plotted in two directions orthogonal to each other is almost same. This was consistent in all the samples tested here; also, the curvature values are consistent among several samples (see Figure 2.5b), suggesting that the film expansion was isotropic and uniform.

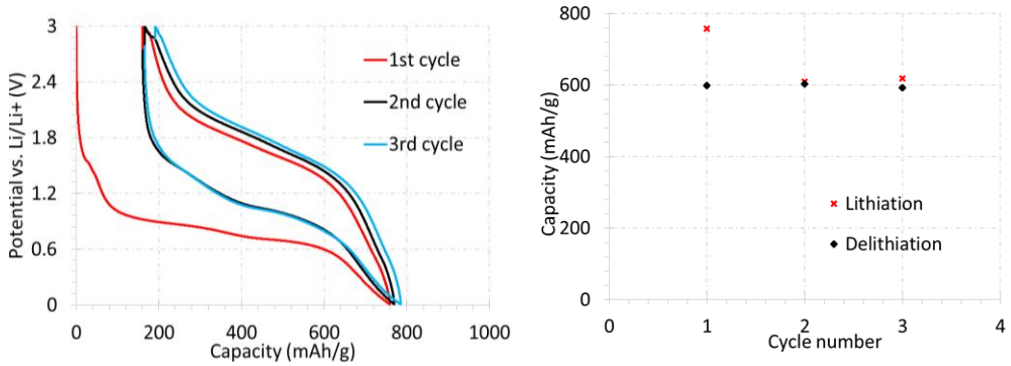

(a) (b)

Figure 2.4 (a) SiO_2 electrode potential as a function of its specific capacity during galvanostatic lithiation/de-lithiation cycling at C/9 rate and (b) shows lithiation/delithiation capacities as a function of cycle number

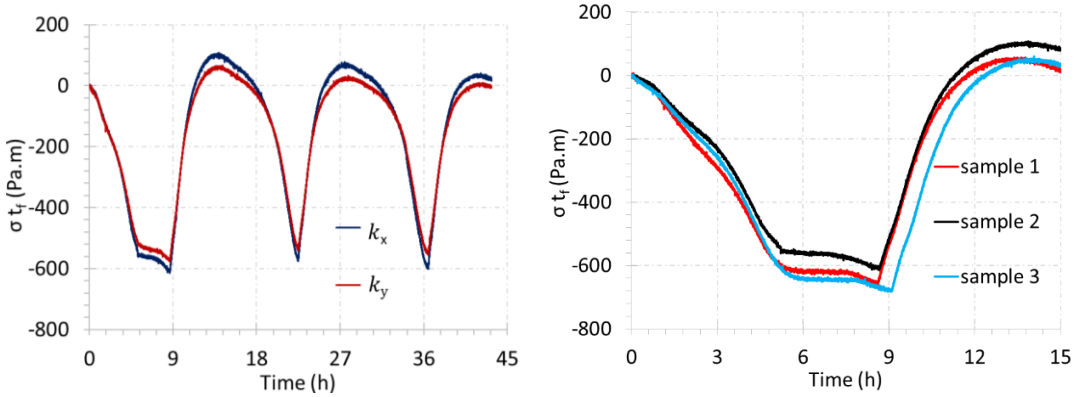

(b) (b)

Figure 2.5 Variation of stress-thickness value (which is proportional to substrate curvature) as a function of time is plotted (a) for two different directions (orthogonal to each other) in a single sample and (b) for three different samples

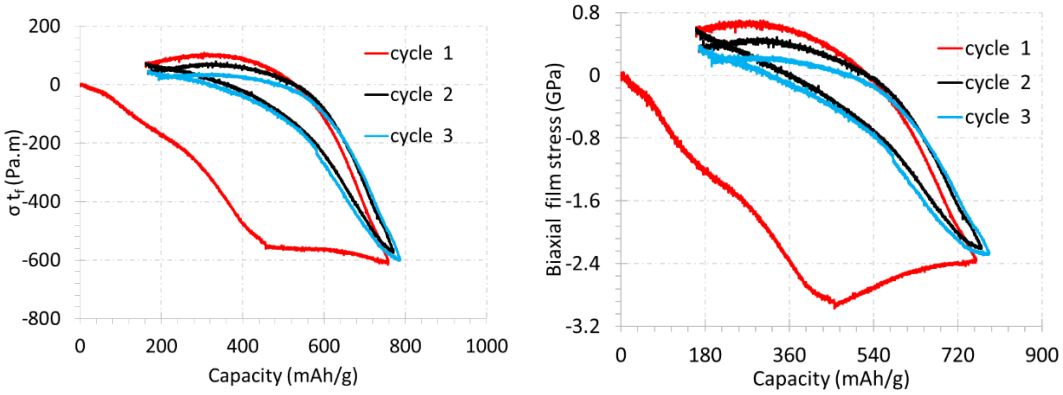

Figure 2.6 Stress-thickness value (or substrate curvature) and biaxial stress in SiO_2 film as a function of specific capacity during galvanostatic lithiation/delithiation at C/9 rate is plotted in (a) and (b), respectively

Figure 2.6b shows the stress in SiO_2 film as a function of capacity during lithiation/delithiation cycling; this is the true stress in the film, calculated based on the stress-thickness data (shown in Figure 2.6a), which is obtained directly from the experiments, and the film thickness, which is calculated from Equation (2.9). Note that the SiO_2 film is subjected to compressive stresses upon lithiation. This is because when the SiO_2 film is lithiated (i.e., lithium insertion into SiO_2 film), the film expands in the thickness direction, i.e., in the direction normal to the plane of the substrate; however, the substrate constrains the in-plane expansion which induces equi-biaxial in-plane compressive stress field in the film. As the lithiation progresses, the compressive stress increases initially with capacity, reaches a peak value of 3.1 GPa at 450 mAh/g, and thereafter decreases to 2.4 GPa at 756 mAh/g. These stress values are significantly higher compared to the tensile strength of pure SiO_2 films (fabricated by PECVD method such as the ones in this study) which is only ~ 0.6 GPa to 1 GPa. [64] Note from Figure 2.6b that the stress increases linearly at low Li concentrations: i.e., below 70 mAh/g capacity and 0.4 GPa of stress, which could be a linear elastic response of the film. Although the pure

SiO_2 is brittle, the lithiated SiO_2 seems to be undergoing extensive inelastic deformation as the stress response beyond 70 mAh/g and 0.4 GPa is non-linear. This suggests that addition of Li to SiO_2 film not only strengthens the film, as it is able to sustain stress values as high as 3.1 GPa, but also makes it ductile so that it can sustain large deformation without fracture. To confirm that the films are intact even after subjecting them to this level (i.e., 3.1 GPa) of stress, SEM analysis was carried out on the samples at different intervals during cycling. Figure 2.7a, 2.7b, and 2.7c show the SEM images of the samples in pristine conditions, after first lithiation and first delithiation respectively. Note that, although there are some morphological changes, the film did not crack during the first lithiation process. This could be attributed to two things: (1) the compressive nature of stress tends to suppress cracking and (2) the lithiated SiO_2 products are tougher than the pure SiO_2. Before performing any electrochemistry, the residual stresses in the SiO_2 films were measured by recording the curvature changes of the substrate before and after SiO_2 deposition. It was observed that the residual stress was only ~80 MPa, which was insignificant compared to the lithiation-induced stress and hence, not included in the plots.

Upon delithiation (i.e., as the Li is removed from SiO_2) the stresses quickly change towards tensile direction. They reach a peak value of approximately 0.7 GPa and decrease with further delithiation. The stress response of the film in the first cycle is completely different from that of the subsequent cycles. This could be due to a combination of different factors such as irreversible reactions (including SEI layer formation), that occur in the first cycle but are absent in the subsequent cycles, and film cracking (which is evident from the SEM images) after first delithiation. The shrinking of the stress-capacity loop and decreasing peak stress also confirm that the film is cracking after the first cycle. It was

reported, [50] e.g., that SiO_2 coatings on Si nanotubes cycled without damage for a few hundred cycles. This can be attributed to the thickness of the films, which is below 20 nm [50] in but 100 nm in this study; in general, thicker films have a higher propensity for cracking. Hence, 100 nm may not be an ideal coating thickness for electrode particles. However, due to size-dependent fracture behavior, sufficiently thin SiO_2 films could sustain stresses as high as 3.1 GPa. It should be noted that although the data presented here provides valuable information that will help in developing electro-chemo-mechanics constitutive models for SiO_2, an in-situ XRD measurement, which is beyond the scope of this work, is necessary to provide a thorough understanding of the SiO_2 mechanical behavior and provides complimentary data to the measured stress data.

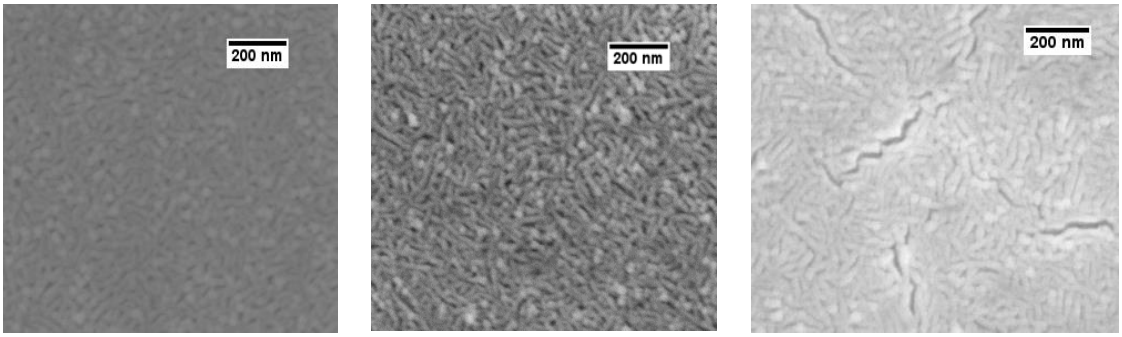

(a) (b) (c)

Figure 2.7 Scanning electron microscope images of (a) pristine SiO_2 film, (b) SiO_2 film after first lithiation, and (c) SiO_2 film after first delithiation. No cracking occurred in the first lithiation process but film starts cracking after first delithiation.

2.3.2 Effect of SiO_2 Mechanical Properties on the Deformation Behavior of Core-Shell Particles Although reports such as [49] showed that SiO_2 coatings on Si particles improved their cyclic performance, one of the obvious questions that remains to be answered is how a brittle coating like SiO_2 sustained a 300% volume expansion imposed by Si without cracking? The stress measurements and observations made in the previous section provide

some clues; i.e., the lithiated SiO_2 products are stronger than pure SiO_2, and they undergo extensive plastic deformation, which generally leads to increased toughness. However, knowledge of the displacement and stress distribution in SiO_2 coatings on Si nanoparticles/nanotubes during electrochemical cycling will provide a more complete picture of how coatings survived hundreds of cycles.

Figure 2.8 shows expansion behavior (normalized radius value at the outer surface) of the Si nanotube as a function of lithium concentration during electrochemical lithiation for three different simulation conditions. As expected, the expansion of bare Si (i.e., filled circles) is the largest at any given lithium concentration, with a final radius to original radius ratio of 1.9 at the end of lithiation. However, the Si nanotube expanded only 1.5 times the original dimension when the SiO_2 layer was modelled as a mechanical clamping layer and expands approximately 1.8 times when the SiO_2 layer was modeled with the measured stress data (concentration dependent yield stress, (Figure 2.6b)). This shows that SiO_2 does provide some clamping effects but the constraint may not be as strong as reported earlier, and the assumption that clamping effect induced by SiO_2 coating promotes mechanical stability of SEI layer needs further investigation.

Figure 2.9a and 2.9b show hoop stress contours of the Si nanotube coated with SiO_2 at the end of lithiation for two different cases: (i) SiO_2 coating was modeled with the measured stress data (ii) SiO_2 coating was modelled as a mechanical constraint layer. It can be observed that when SiO_2 coating is assumed as a pure mechanical clamping layer with elastic-plastic properties [13], the hoop stress in SiO_2 reaches as high as 2.9 GPa, which is significantly higher tensile stress than the fracture strength of SiO_2, which could lead to cracking. However, when SiO_2 is modeled using the measured stress response, the peak

stress in SiO_2 at any stage of lithiation is less than 0.41 GPa, which is lower than the fracture strength of SiO_2. This clearly provides a plausible explanation as to why the coatings reported in earlier studies [49] were able to sustain a 300% volume change of Si for several cycles. Further, the stresses in Si particles are also relatively less when measured properties of SiO_2 are used in the model. In addition to the inelastic nature of lithiated SiO_2 and stronger lithiated products as mentioned earlier, these FE results show that the lower hoop stresses in SiO_2 and Si were probably the reason for superior performance of Si/SiO_2 nanotubes in [49]. Therefore, it is important to incorporate the measured electrochemical and stresses response while developing electro-chemo-mechanics models of SiO_2, which will be used to design complex SiO_2 coated Si electrode architectures.

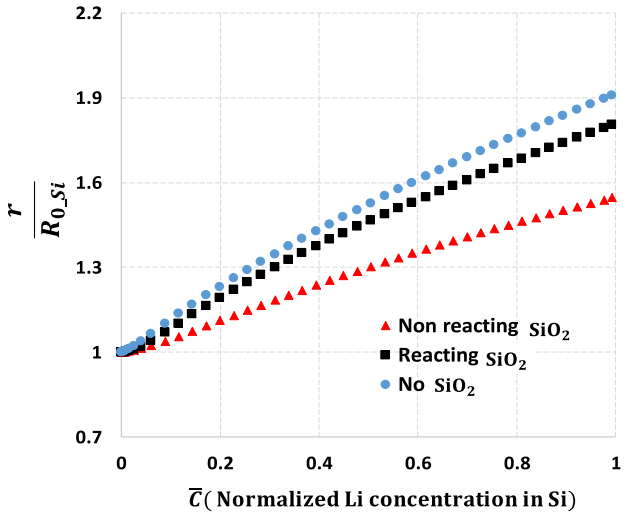

Figure 2.8 Evolution of normalized radial displacement at the outer surface of Si nanotube as a function of Li concentration during lithiation for 3 different cases: (i) filled circles represent the baseline expansion behavior of Si nanotube without SiO_2 coating, (ii) filled triangles represent a case where SiO_2 coating was modeled as elastic-plastic mechanical constraint layer which allows Li^+ to diffuse (such as an artificial SEI), and (iii) filled squares represent a case where SiO_2 was modeled as per the measured stress response.

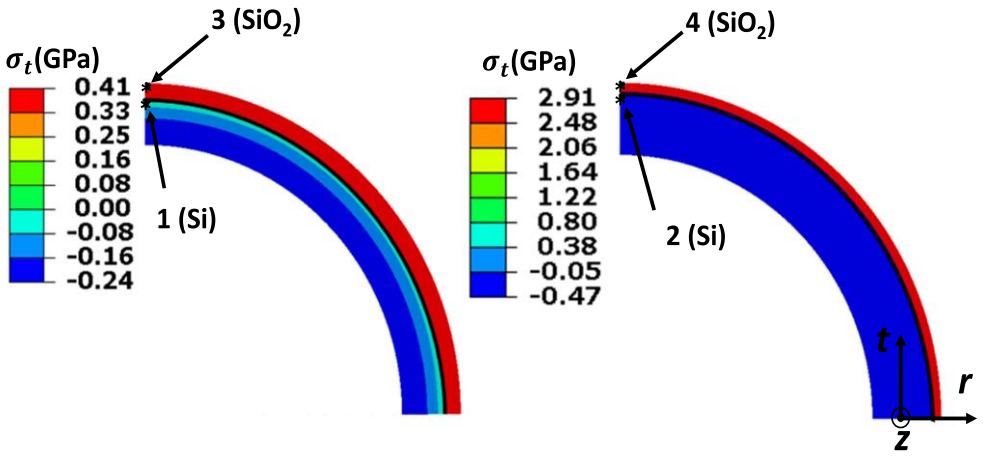

Figure 2.9 Contours of hoop (or circumferential) stress component at the end of lithiation in Si nanotube coated with SiO_2 (a) when SiO_2 coating was modeled as per the measurements in section 4.1 and (b) when SiO_2 modelled as elastic-perfectly plastic mechanical constraint layer.

2.4 Conclusions

To be able to provide mechanistic explanation as to how highly brittle SiO_2 coatings on Si were able improve the cyclic performance of Si by sustaining 300% volume expansion for several hundred cycles, a simple finite element model of SiO_2-coated Si nanotube (core-shell type microstructure) was developed; the SiO_2 coating was modeled using measured stress and electrochemical response. It was observed that the clamping action provided by SiO_2 is relatively lower than was reported in the literature, which suggests that the current understanding of clamping effects of oxide coatings providing stable SEI needs to be investigated further. Also, it was observed that the maximum stress in the SiO_2 coating during electrochemical cycling (i.e., under 300% volume change of Si) is approximately 0.41 GPa, which is less than the fracture strength of pure SiO_2 films, providing a plausible explanation as to why oxide coatings survived several hundreds of cycles without failure.

This observation along with the stress measurements suggests that the addition of Li to SiO_2 film not only strengthens the film, as they are able to sustain stress values as

high as 3.1 GPa, but also makes it ductile so that it can sustain large deformation without fracture. In addition to the above insights, the results and observations made in this study are also useful (i) to develop a comprehensive electro-chemo-mechanics models of SiO_2 films and (ii) to design and develop next generation SiO_2 coating-based core-shell type of microstructures for electrodes that are mechanically and chemically stable. Finally, the battery electrodes based on Si will have a thin layer of native oxide film on all the particles, and it is important to understand the electrochemical and mechanical properties of the oxide layer for which a basic preliminary understanding was given in this study.

CHAPTER 3

IN SITU MEASUREMENT OF THE EFFECT OF STRESS ON THE CHEMICAL DIFFUSION COEFFICIENT OF LI IN HIGH-ENERGY-DENSITY ELECTRODES

3.1 Introduction to Li Diffusivity

Solid-state diffusion of lithium through active material (in anodes and cathodes) is a crucial aspect of lithium-ion battery operation. For example, during charging of a battery, Li-ions diffuse through the bulk of a cathode particle (usually a transition metal oxide) to reach the particle/electrolyte interface, and they get transported across the electric double layer to enter into electrolyte solution where they diffuse in the electrolyte solution towards anode; the ions then get transported across the double layer to hop onto the anode surface and diffuse through its bulk; simultaneously, electrons travel from cathode to anode through an external circuit to maintain charge neutrality. This entire process proceeds in the opposite direction during discharging. As the diffusion coefficient of Li^+ in liquid electrolyte is several orders of magnitude larger than that in solid active materials, and assuming that the interfacial ion transfer is fast, the rate-determining step in lithiation/delithiation process, in general, is the Li-ion diffusion in bulk of electrodes. Further, the solid-state diffusion phenomenon will be increasingly critical for all solid-state lithium-ion batteries. [65-66] The ease of Li^+ diffusion allows efficient use of active material available in electrodes, enhancing the overall performance of a battery, i.e., high specific capacity at high charge/discharge rates. Hence, the transport kinetics of lithium in electrodes not only dictate the power density but also the energy density of a battery.

Quantitative information about the transport phenomenon is essential to understand diffusion mechanisms and designing effective electrode architectures to optimize the power density and energy density of electrode materials. For example, mathematical models which attempt to simulate a range of physics from only electrochemistry to coupled electrochemistry [67-68] and mechanics, [12][17][37-38][69] rely on Li-ion diffusivities in active materials to predict key electrode characteristics such as charge/discharge rates, open circuit potentials, intercalation kinetics, and electrode stresses. Hence, reliable and accurate transport properties are critical for these models to accurately simulate battery operations either at a particle level or at an overall battery level for effective optimization of electrode microstructures. A precise method of diffusion coefficient measurement not only provides these properties but is also necessary to characterize the transport behavior of emerging electrode materials.

A large number of studies have been published on various methods which can provide transport properties of electrodes; among them, the transient electrochemical techniques developed by Weppner et al.[70] and Wen et al.[33] the galvanostatic intermittent titration technique (GITT) and the potentiostatic intermittent titration technique (PITT) are the most widely used methods. These methods, which assume a simple Fickian diffusion model, were originally proposed for linear slab geometries (i.e., solid thin film electrodes) and were later modified to measure transport properties in various anode and cathode materials both in thin film and composite electrode configuration. [6][8][71-75]

Despite numerous modifications to PITT and GITT, [6][8][71-75] none of the studies considered electrode stresses and the effect of stresses on the measured chemical

diffusion coefficient. In other words, the above studies ignored the stresses in electrodes during electrochemical reactions. However, it is known that all the electrode materials experience mechanical stresses during electrochemical reactions: some to lesser extent and the others to a greater extent. For example, graphite which expands about 10% when fully lithiated is shown to experience a peak stress of -0.25 GPa, [76] but most of the high energy density (typically large volume expansion) electrodes such as Si, [11][61][77] SiO_2, [78]Sn,[79] and Ge[14][80] are subjected to stresses greater than 1 GPa during electrochemical reactions. It was also shown that this level of stresses could influence the open circuit potential of an electrode [81-82] and lithiation/delithiation kinetics; hence, they may affect the transport of Li ions in electrodes. [83-84] Hence, it is important to understand and quantify how the stresses in electrodes evolve during the diffusion coefficient measurement process (e.g. GITT and PITT), especially in large volume expansion electrode materials. Also, it is important to quantify the effect of stress on transport, because this could have implications on the fracture of electrode materials [85] and reaction kinetics of the electrodes. [83-94][86-88]

The primary objectives of this study are:

1) To understand how the stresses in electrodes evolve during GITT and PITT experiments, and to identify which one of these methods will be suitable for large volume expansion materials; and

2) To understand and quantify the effect of stress on the chemical diffusion coefficient of Li in large volume expansion electrode materials.

To this end, sputter deposited Ge nano-films have been selected as a model electrode to achieve the objectives. The Ge thin film electrodes were assembled in a half-cell configuration with a thin foil of lithium as a reference/counter electrode. The electrodes

were separated by a Celgard polymer separator. The planar thin film electrodes used here eliminate both geometrical and material complexities involved in the diffusion analysis of composite electrodes with complex shaped particles, binder, and conductive additives. Thin solid films are not only suitable for accurate stress measurements but are also ideal for fundamental electrochemical and transport property characterization. The Ge films in the half-cell were subjected to series of GITT and PITT protocols to measure the chemical diffusion coefficient as a function of Li concentration while simultaneously measuring the stresses in the electrodes using substrate curvature technique. It was observed that the chemical diffusion coefficient not only changes with Li concentration but is also a strong function of electrode stresses.

3.2 Experimental Methods

3.2.1 Ge Thin Film Electrode and Electrochemical Cell Preparation The electrodes were prepared by depositing 5 nm of Ti (adhesive layer) and 200 nm of Cu (current collector) followed by a 100 nm of Ge on a 2-inch double side polished fused silica wafer (525 μm thick, and 50.8 mm diameter). The fused silica wafer serves as an elastic substrate for the purposes of curvature-based stress measurements, and it does not participate in the electrochemical reactions. The films were deposited by DC sputtering at a working pressure of less than 3 mTorr Ar while the base pressure before introducing the Ar gas was 4.4×10^{-6} Torr. Ge thin films sputter deposited under these conditions are known to be amorphous.[14] The residual stresses developed in the Ge film due to the deposition process was measured by tracking the curvature changes of the substrate before and after the Ge film deposition.

Li-ion half cells were assembled and tested in an argon-filled glove box (maintained at 25°C and with less than 0.1 ppm of O_2 and H_2O). The Ge thin film was used as working electrode and lithium foil (1.5 mm thick, 99.9 % metal basis from Alfa Aesar) as counter/reference electrode, with a Celgard polymer separator preventing physical contact between the electrodes; the staking and orientation of the electrodes in the beaker cell is shown in previous chapter (Chapter 2) in Figure 2.2. The electrolyte, a 1 M $LiPF_6$ in 1:1:1 ratio (by wt%) of (EC) ethylene carbonate: (DEC) diethyl carbonate: (DMC) dimethyl carbonate (Selectilyte A2 series from BASF) was added to the beaker such that the lithium foil, Celgard polymer separator and Ge film were submerged in the electrolyte but the back surface of the elastic substrate was not submerged. This was done to prevent the laser from traversing in the electrolyte solution. A glass window was used to provide optical access to the sample as well as to seal the cell. Planar thin film electrodes were selected to avoid geometric and material (i.e., binder and conductive additives) complexities associated with composite electrodes. A planar thin film configuration provides ideal conditions not only for studying/characterizing the diffusion phenomenon in electrodes (as the problem reduces to 1D diffusion) but also for measuring stress during electrochemical cycling.

3.2.2 Electrochemical Measurements Solartron 1470 E potentiostat was used to perform electrochemical experiments. Ge thin film electrodes were lithiated/delithiated under a constant current density of 5 $\mu A/cm^2$ between 1.2 V vs. Li/Li^+ (or open circuit potential) and 0.05 V vs. Li/Li^+, similar to an earlier report. [14] This was done to measure the baseline stress response of Li_xGe film as a function of Li concentration. In the PITT experiments, Ge thin film electrodes were lithiated at a constant current density of 5 $\mu A/cm^2$ (which corresponds to C/17.5 rate) until the potential dropped down to 0.4 V vs

Li/Li^+ before applying a PITT protocol. When the film reached 0.4 V vs. Li/Li^+, a step change of 50 mV was applied (i.e., to reach a new potential of 0.35 V vs Li/Li^+) and it was held constant until the current decays to 0.25 $\mu A/cm^2$. A sequence of these PITT protocols each resulting in a 50 mV decrease were carried out until the electrode potential dropped to 0.05 V vs Li/Li^+. Lithiation below 0.05 V vs Li/Li^+ was prevented to avoided any phase change behavior of Li_xGe.[14] The film was then delithiated with a sequence of 50 mV vs Li/Li^+ step increases until the potential reached 1.2 V vs Li/Li^+ with a potential hold at each step until the current dropped to 0.25 $\mu A/cm^2$. Throughout this experiment (i.e., all the PITT protocols during lithation and delithiation), the stress response and the current response of the film was recorded. In the GITT experiments, a single titration step consisted of galvanostatic lithiation at a current density of 5.72 $\mu A/cm^2$ for 15 minutes followed by a relaxation step for 120 minutes. This protocol was continued until the potential of the electrode reached 0.05 V vs. Li/Li^+, which resulted in a sequence of 15 GITT steps during lithiation. A similar process was followed during delithiation with 15 GITT steps. Throughout this experiment, the stress response and the potential response of Ge film was recorded. At least 3 fresh specimens were tested in each case (i.e., 3 samples for GITT, 3 samples for PITT, and 3 samples for galvanostatic experiment were measured), and all the samples tested in this study were cycled above 0.05 V vs. Li/Li+ to prevent amorphous to crystalline transformation of lithiated Germanium. [14][89]

3.2.3 In situ stress measurements Stress response of amorphous Ge (a-Ge) thin film during the electrochemical cycling was measured by monitoring the substrate curvature with MOS setup (k-Space Associates, Dexter, MI) illustrated in Figure 2.2 of Chapter 2.

Although there are no well-controlled direct experiments on the volume expansion behavior of Ge during electrochemical cycling, Liang et al. [86] showed from a transmission-electron microscopy that Ge nanoparticles expanded up to 260% upon complete lithiation. As the elastic substrate constrains the Ge film (i.e., a constant area) in the current experiments, the volume change mainly occurs due to thickness change. Hence, a linear relation between film thickness, t_f, and state of charge (SOC) is assumed as follows,

$$t_f = t_f^0(1 + 2.6m) \tag{3.1}$$

where t_f^0 is the initial film thickness and *m* is state of charge which varies between 0 and 1. *m* =1 corresponds to full capacity (1625 mAh/g) and a volumetric strain of 2.6. [86]

3.3 Results and discussion

3.3.1 Stress Evolution during Galvanostatic, PITT, and GITT Experiments Figure 3.1a and 3.1b show the variation of potential and biaxial film stress, respectively, as a function of lithium concentration in Ge film during a galvanostatic lithiation/delithiation process. Upon lithiation the potential of the film drops sharply from an open circuit value of ~3.0 to 0.5 V vs. Li/Li^+ and decreases gradually thereafter with the Li concentration to a value of 0.05 V vs. Li/Li^+. This indicates that the lithiation of Ge film started approximately at 0.5 V vs. Li/Li^+. Upon delithiation, the potential rises quickly to 0.25 V vs. Li/Li^+ and thereafter it increases gradually with decrease in lithium concentration until $x < 1$ (i.e., at low lithium concentration values) at which the potential starts to rise quickly. The absence of flat regions in the potential curve (both during lithiation/delithiation)

suggests that the sputtered a-Ge film remains amorphous Li_xGe throughout the lithiation/delithiation cycling, i.e., addition (or removal) of Li to amorphous Ge leads to an amorphous Li_xGe alloy (a homogeneous solid solution). This behavior is similar to that observed in previous reports on Ge electrode. [14][88][90]

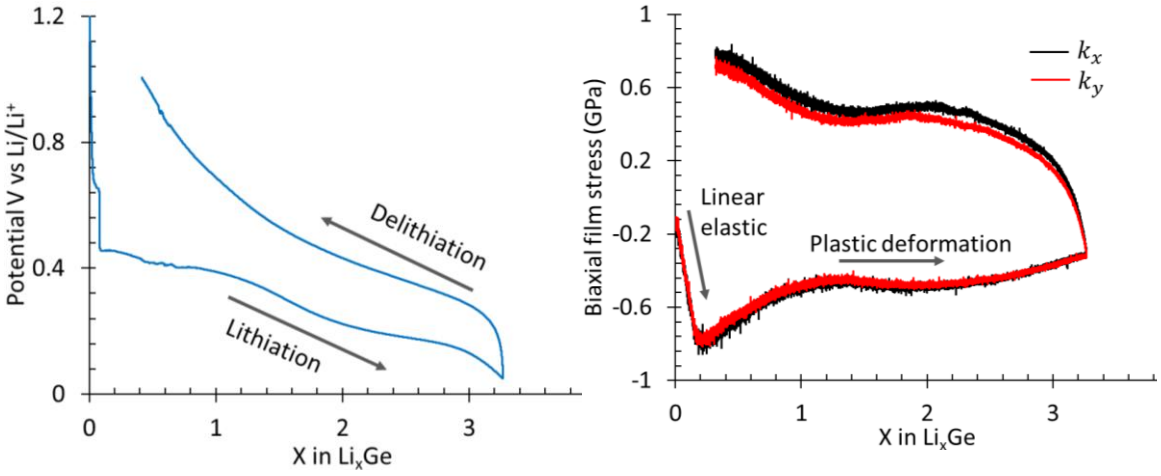

(a) (b)

Figure 3.1 (a) and (b) show potential and stress, respectively, as a function of lithium concentration (i.e., x in Li_xGe) during galvanostatic lithiation/delithiation.

Figure 3.1b shows that the stress in the Ge film is non-zero (- 0.134 GPa) at zero lithium concentration (i.e., at x= 0), which is due to the residual stresses in the film. In general, depending on the thermal expansion coefficient properties of film/substrate system, thin films have residual stresses due to relatively high temperature deposition process (magnetron sputtering) followed by subsequent cooling to room temperature. The residual stresses in the present Ge samples varied from -0.134 to -0.243 GPa. During lithiation, i.e., when lithium enters the Ge film, the in-plane (i.e., x-y plane) expansion of the film is constrained by the rigid elastic substrate (i.e., fused silica, see Figure 3.1b) resulting in biaxial compressive stress in the film; the film expands freely in the out-of-

plane (or z) direction. The red and black curves in Figure 3.1b represent the stress data corresponding to two different directions (x and y), orthogonal to each other; the fact that the stress values are almost same in both directions at any given lithium concentration means that the film expansion is isotropic and proves that the stress state is equi-biaxial.

Note from Figure 3.1b that, initially, the compressive stress (indicated by negative value) increased linearly with Li concentration to a peak value of -0.8 GPa (at x= 0.2, i.e., $Li_{0.2}Ge$); with further lithiation, the stress response becomes non-linear (at x = 0.2) and decreases to -0.5 GPa (at x= 1, i.e., LiGe). The stress remains almost constant at -0.5 GPa for the major portion of lithiation but decreases to -0.34 GPa at the end of lithiation. The initial linear stress response of the film is attributed to the elastic response, but as the lithium concentration increases beyond 0.2, i.e., x > 0.2, Li_xGe starts to undergo plastic deformation resulting in non-linear response; the plastic deformation continues until the end of lithiation. Upon delithiation, the stress increases rapidly and becomes positive (i.e., tensile stress) within a small decrease in lithium concentration; this rapid linear increase due to removal of lithium from the film is due to elastic unloading of the film, which can occur at any lithium concentration. Note that elastic unloading leads to significant changes in stress with small changes in lithium concentration. With further delithiation, the stress response becomes non-linear (i.e., plastic deformation) at 0.3 GPa, increases slightly to 0.5 GPa, and remains almost constant before increasing as Li concentration decreases below 1 (or x < 1), mirroring the stress response during lithiation process. These observations agree with those reported in previous reports. [14][80][91] It should be noted that the stress values presented in the Figure 3.1b should be thought of as the yield stress of Li_xGe as a function of Li concentration. This is the basic information that one needs to be able to

simulate the coupled large deformation kinematics and electrochemistry of battery electrodes. [12][38][92-93]

The standard GITT or PITT analysis for evaluating diffusion coefficient ignores electrode stresses or change in stress in a given titration step. To be able to use a similar approach, one should make sure that the change in electrode stresses during a single titration step (either in PITT or GITT) must be negligible. Hence, it would be ideal to conduct the titration steps when the electrode undergoes plastic deformation (i.e., for $x > 1$ during lithiation and $x < 3$ during delithiation in Figure 3.2b), because in this region stress remains almost constant with Li concentration as long the elastic unloading of the film (i.e., either removal of lithium from electrode during lithiation process or adding lithium to electrode during delithiation process) is prevented. Figure 3.2b shows the prescribed potential steps (blue) and the corresponding current response of the film (red) in a PITT experiment. Note that the Ge film was lithiated galvanostatically until it starts deforming plastically (0.4 V vs. Li/Li^+ or $x > 1$) before applying PITT protocols. It can be observed that during the potential holds, the current decays exponentially from an arbitrarily large value at the beginning of the titration step (due to sudden increase of potential) to a negligibly small value at the end, but in each titration step the electrode is continued to be lithiated (or delithiated) which prevented elastic unloading.

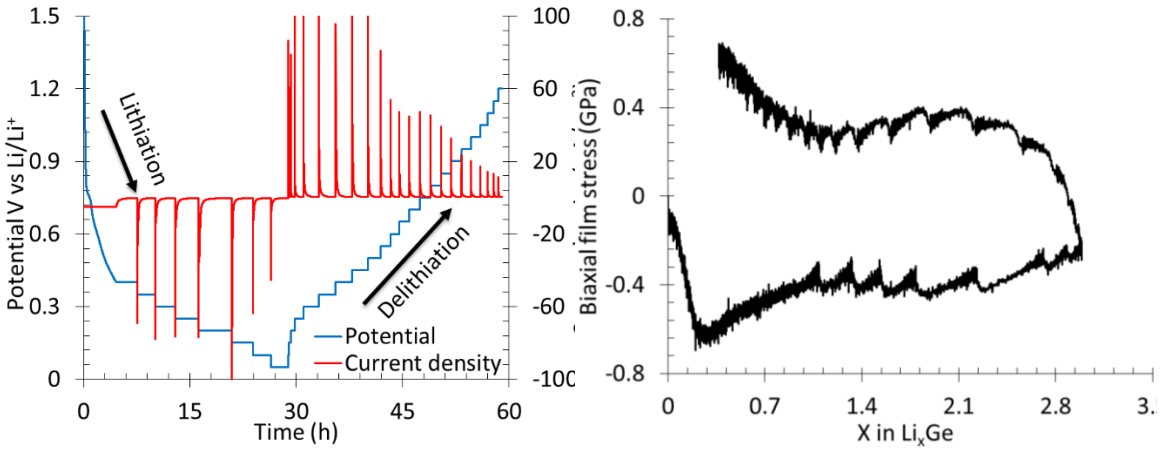

(a) (b)

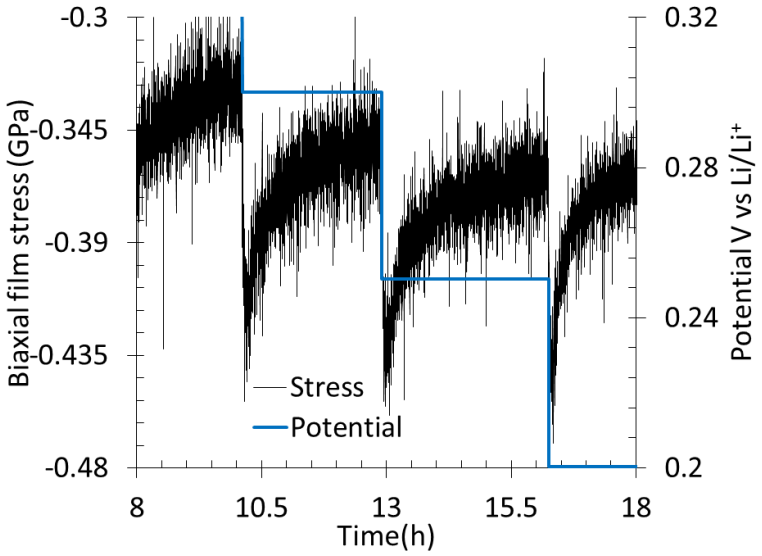

(c)

Figure 3.2 (a) Shows the current response of the Ge film (in red) to the applied step potentials (in blue) during a PITT experiment, (b) shows the stress evolution as a function of lithium concentration due to the prescribed potential history, and (c) shows that typical stress change (increase/decrease) in a given titration step is between ~80 to 90 MPa during PITT protocols.

Figure 3.2b shows the evolution of electrode stress as a function of lithium concentration in response to the prescribed potential history showed in Figure 3.2a. Note that the overall stress response of the film as a function of lithium concentration is similar

to that showed in Figure 3.2b, but there is a slight variation in the electrode stress in a single titration step; a zoomed in view of stress and potential variation in a typical PITT titration step is shown in Figure 3.2c for clarity. Although the lithium concentration was increasing monotonically, which should have resulted in almost constant stress (for $x > 1$ according to Figure 3.2b), the stress changed slightly within a given titration step, with some potential holds resulting in a stress change of 60 MPa and others 90 MPa. This stress variation can be attributed to the strain-rate sensitivity of the lithiated Ge film. Nadimpalli et al. [14] and Pharr et al. [80] showed that the stresses in lithiated Ge film are not just the function of lithium concentration but are also functions of lithiation/delithiation rate (or strain-rate). In other words, besides lithium concentration, the electrode stress may weakly (or strongly) depend on the applied current, with higher current densities (or higher strain-rates) generally resulting in higher electrode stresses; for example, note from Figure 3.2c that the stress response in a single potential hold mimics (qualitatively) the exponential decay in current. A highly rate sensitive (rate-insensitive) material compared to Li_xGe would have resulted in more (less) than 90 MPa of stress change in a single titration step if subjected to the exact loading history shown in Figure 3.2a.

Figure 3.3a, 3.3b, and 3.3c show the prescribed electrochemical loading history, variation of stress as a function of lithium concentration, and the details of stress evolution in individual titration steps, respectively, in GITT experiments. A total of 15 titration steps during lithiation and 15 steps during delithiation can be seen in the Figure 3.3a. In a single titration step, a constant current (i.e., constant flux, denoted by red curve) was prescribed for a small amount of time followed by an open circuit condition to let the electrode potential (or Li concentration) relax towards its equilibrium potential (equilibrium Li

concentration). The potential relaxation as a function of time is due to transport of Li through Ge electrode; by modeling this transport process using a simple Fick's law, transport properties such as diffusion coefficients were obtained for several electrode materials. [72][74-75][94-98] However, Figures 3.3b and 3.3c show that the electrode stresses in lithiated Ge tend to relax towards an equilibrium value during the potential relaxation, which resulted in a change in stress as high as 0.5 GPa in a single titration step during the GITT experiments. This is a significant change compared to that observed in the PITT experiments (Figure 3.2c) and too big to be ignored in the diffusion analysis for diffusion coefficient measurement.

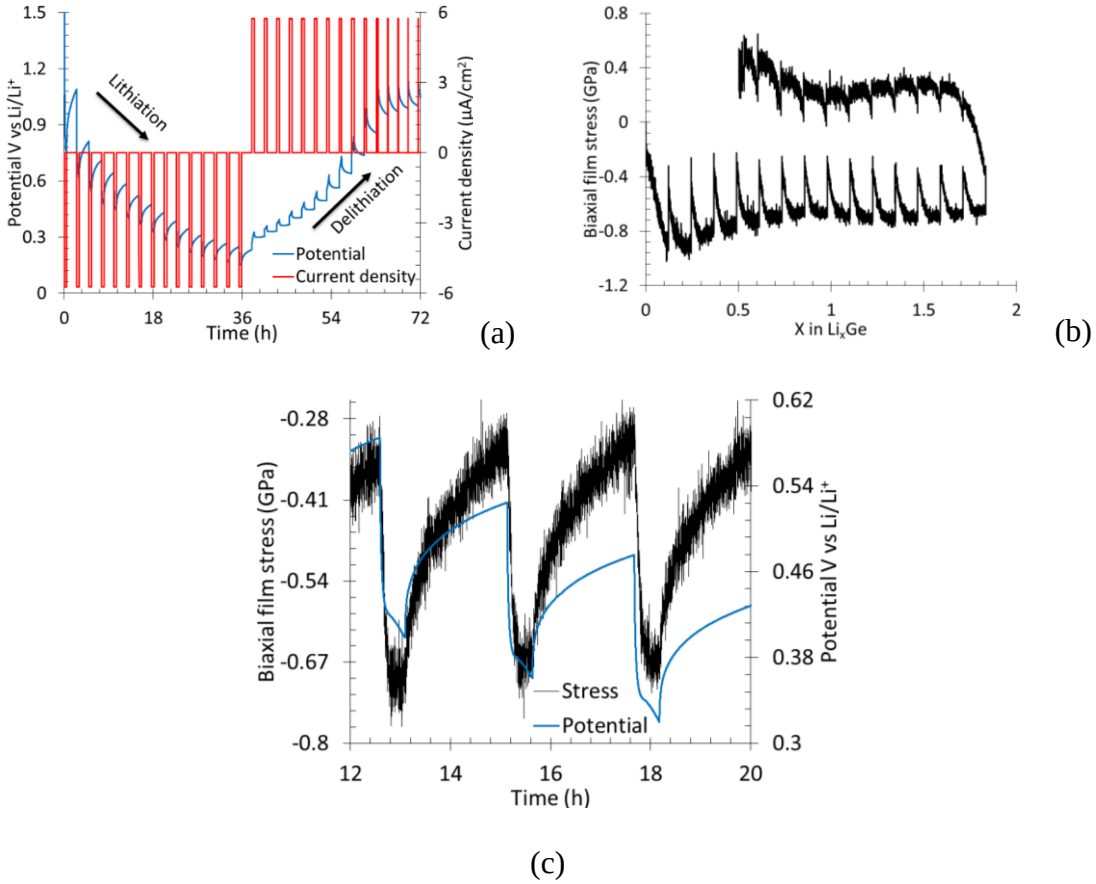

Figure 3.3 (a) Shows the potential response of Ge thin film electrode (in blue) to the applied step currents (in red) during a GITT experiment, (b) shows the stress evolution as a function of lithium concentration due to the prescribed current history, and (c) shows that typical stress change (increase/decrease) in a single titration step is ~350 MPa to 500 MPa.

Hence, for electrode materials such as Ge, and other similar large volume change materials (Si, Sn, Al, and their alloys), the stress changes in a GITT experiment may be significant; therefore, the analysis based on simple Fickian diffusion model for evaluating chemical diffusion coefficient may lead to errors. An elaborate transport model with multiphysics material behavior which couples large deformation plasticity along with electrochemisty, such as the model as presented by Bucci et al. [12][99] may be required. However, if the electrode material such as Ge in Figure 3.2 is not a strong rate sensitive material, stress change during a single titration step in PITT is significantly smaller, and the analysis method based on simple Fickian model can be employed with relatively low error. It is instructive to use a simple model to understand how the chemical diffusion coefficient will be affected by the concentration and stress in a solid active material.

3.3.2 Effect of Stress on Chemical Diffusion Coefficient As the variation of stress in a single titration step was considerably large in GITT experiments, only the data from PITT experiments was analyzed to obtain the chemical diffusion coefficients. The schematic in Figure 3.4 illustrates the one-dimensional transport of Li^+ in Ge thin film considered here and defines various parameters used in the model. Similar to Ref., the chemical diffusion process of Li in Ge thin film is assumed to obey 1D Fick's law,

$$\frac{\partial c}{\partial t} = \widetilde{D}\frac{\partial^2 c}{\partial z^2} \tag{3.2}$$

where c and $\widetilde{D}$ are concentration and the chemical diffusion coefficient of Li^+ in germanium, respectively; t is time (s) and z is the coordinate (representing out-of-plane direction) defined in Figure 3.4. As mentioned earlier, the ion transfer kinetics at the

interface and the diffusion of Li-ions in the electrolyte are assumed to be significantly faster than the diffusion of Li-ion through Ge film, which is a reasonable assumption. Also, the solid electrolyte interphase formation at the Ge film and electrolyte interface (i.e., at z = 0 in Figure 3.4) is neglected.

The flux of Li^+ (i.e., current) required to maintain a constant potential (i.e., a constant concentration of Li^+ on the electrode surface) in a PITT step can be obtained by solving the Equation (3.2) with boundary conditions shown in Figure 3.4. The solution to this problem, i.e., the current as a function of time in the long-time duration approximation ($t >> t_f^2 / \widetilde{D}$) is,

$$I(t) = \frac{2Q\widetilde{D}}{t_f^2} \exp\left(-\frac{\pi^2 \widetilde{D} t}{4t_f^2}\right) \tag{3.3}$$

where t_f is electrode thickness (cm), obtained according to Equation (3.1), and Q is the charge accumulated (or lost) in a single titration step estimated as,

$$Q = \int_0^t I(t)dt. \tag{3.4}$$

It can be noted that taking the natural logarithm on both sides of Equation (3.3) will result in the following equation for a straight line,

$$\ln(I) = \ln\left(\frac{2Q\widetilde{D}}{t_f^2}\right) - \left(\frac{\pi^2 \widetilde{D}}{4t_f^2}\right) t, \tag{3.5}$$

with $\ln\left(\frac{2Q\widetilde{D}}{t_f^2}\right)$ as the y-intercept and $\left(-\frac{\pi^2 \widetilde{D}}{4t_f^2}\right)$ as the slope;[33] the chemical diffusion coefficient $\widetilde{D}$ can be evaluated from either the intercept or the slope. As per Wen et al., [33] both approaches should result in similar $\widetilde{D}$ values, which is what we have observed for few

calculations that were performed for one case during delithiation. Hence, we chose the slope method for our case as it eliminates additional calculations (Equation (3.4)) of estimating *Q*.

Figure 3.5 shows the ln (*I*) as a function of time of the data from a typical titration step in the PITT experiment (dotted line) along with a linear fit (Equation (3.5)) to the data; the fit is considered good if R^2 > 99.5. As expected, the experimental data agrees reasonably well with Equation (3.5) at longer times (i.e., at later stages of diffusion in a titration step) but not at the beginning of the potential step, because Equation (3.5) was obtained for long-time approximation. The slope value from the fit at each titration step and the film thickness t_f are then used to determine the $\widetilde{D}$ at any given Li concentration and electrode stress level. Note that the film thickness changes slightly during the titration step; hence, the average of thickness at the beginning and at the end was used in the estimation of $\widetilde{D}$.

Figure 3.6a shows the variation of chemical diffusion coefficient $\widetilde{D}$ as a function of electrode stress and lithium concentration obtained from the PITT experiment corresponding to Figure 3.2. The solid line with filled circles corresponds to the $\widetilde{D}$ values obtained during lithiation process whereas the line with filled triangles represents the data obtained during delithiation; the stress state during lithiation and delithiation (at any concentration) is given by the thick solid black curve. Note that the $\widetilde{D}$ increases significantly with Li concentration both during lithiation and delithiation; for example, it increases from a value of 30 X 10^{-15} cm^2/s at x = 0.1 to a value greater than 150 X 10^{-15} at x > 3.1 during delithiation. In addition, the $\widetilde{D}$ values obtained during lithiation are smaller than those obtained from the delithiation process at any given lithium concentration, and

the difference (or offset in $\widetilde{D}$ at any particular concentration) increases with concentration. For example, at x =1.4, the $\widetilde{D}$ values obtained during delithiation are twice the value obtained during lithiation, and the delithiation values becomes four times more at x = 2.8. These observations are consistent among the data obtained from three different samples, see Figure 3.6b. The $\widetilde{D}$ values obtained here are a couple of orders of magnitude lower than those reported by Laforge et al. [88] which could be attributed to the differences in their sample configuration and measurement method. However, the measured diffusion coefficient values of Li in Ge are higher than those obtained in Si, suggesting that Ge will offer a better rate capability (i.e., power density) than the Si electrodes which is in agreement with the previous studies.[88-89]

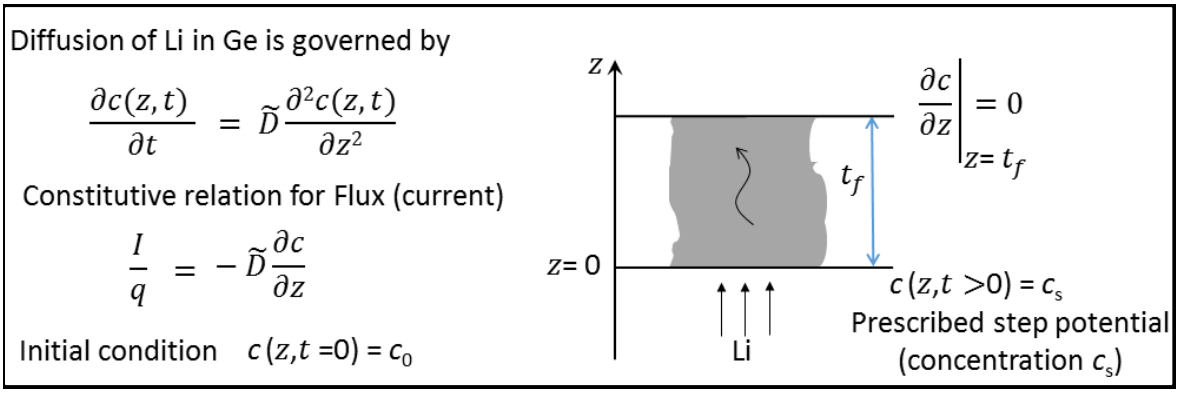

Figure 3.4 Schematic of the one-dimensional chemical diffusion of Li-ion in germanium thin film electrode (according Fick's law) with $z = 0$ representing the interface between the Ge film and the electrolyte. t_f is the thickness of lithiated Ge film at a given state of charge as per Equation 3.1.

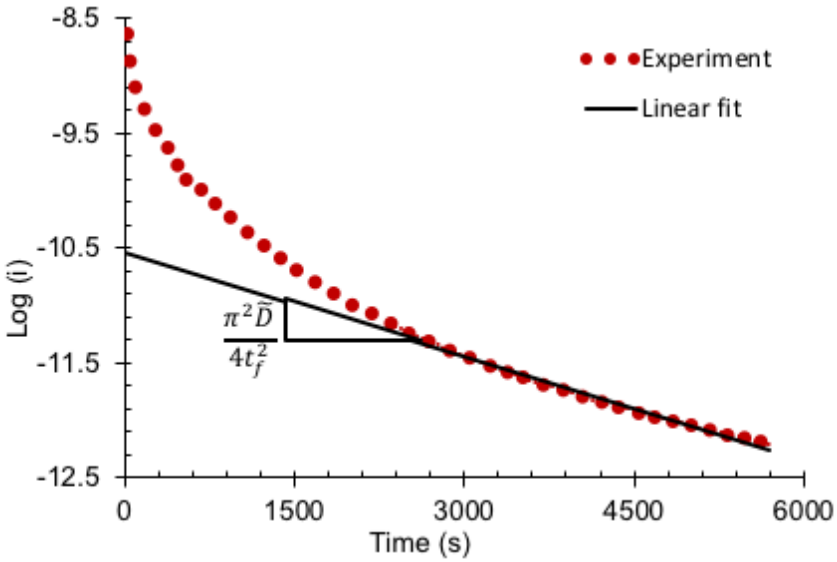

Figure 3.5 Variation of logarithm of current plotted as a function of time in a typical titration step (during PITT). The linear fit of Equation (3.5) to the data agrees well at the longer time, i.e., at $t >> t_f^2 / \widetilde{D}$.The slope of the curve provides the information necessary for evaluating $\widetilde{D}$.

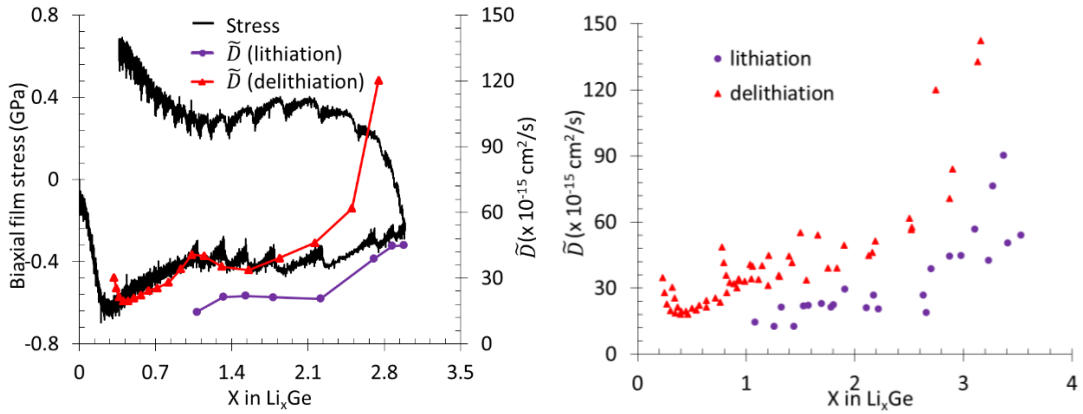

(a) (b)

Figure 3.6 (a) Chemical diffusion coefficient $\widetilde{D}$ and stress plotted as a function of lithium concentration during a PITT experiment, and in (b) the $\widetilde{D}$ values obtained from three different samples are shown. Note that $\widetilde{D}$ increases with Li concentration in all the samples, and the tensile stresses enhance while compressive stresses impede Li transport.

The boundary conditions corresponding to a PITT experiment are also shown. According to Wepner and Huggins, [70] the chemical diffusion coefficient $\widetilde{D}$ is given by

$$\widetilde{D} = D\,W \tag{3.6}$$

where W is an enhancement factor (which contains contributions from thermodynamic and mechanical factors) and D is the component diffusion (or intrinsic-diffusion) coefficient. Using a chemical potential that takes into account the electrode stresses in addition to Li concentration, Bucci et al. showed that the enhancement factor in the above equation can be given as,

$$\frac{\widetilde{D}}{D} = W = \left[\frac{c_{max}}{c_{max}-c} + \frac{\partial \ln \gamma}{\partial \ln c}\right] + \frac{c}{RT}\frac{\partial \mu}{\partial \sigma}\frac{\partial \sigma}{\partial c} \tag{3.7}$$

where c_{max} is the maximum value of Li concentration (which is 3.75 for Ge), γ the activity coefficient (which approaches 1 as c approaches 0), μ the chemical potential. The R and T are universal gas constant (8.314 J/mol. K) and temperature (T=298 K), respectively. The first two terms (with in square brackets) in the equation are chemical contribution to the diffusivity enhancement and the remaining term is the contribution from mechanical stresses in the electrode. It is instructive to make first order estimates of the relative contributions from chemical and mechanical terms to the enhancement factor given in Equation (3.7). The procedure for evaluating γ is not trivial and described in Verbrugge et al,[100] Bucci et al;[12] however, for very low lithium concentrations, it is reasonable to assume γ to be 1. Consequently, only one term in the square brackets remains. Using the Larché-Cahn theory Sethuraman et al. [82] have derived stress-potential coupling for a thin Si film electrode; following the same approach for Ge film in this study, the stress-chemical

potential coupling term is given as:

$$\frac{\partial \mu}{\partial \sigma} = \frac{2\,\nu_{Ge}\eta}{3} \tag{3.8}$$

where, μ is the chemical potential, ν_{Ge} is the partial molar volume of Ge, η is the rate of change of volumetric strain (ε_v) in the Ge electrode due to lithiation, defined as $\eta = \frac{d\varepsilon_v}{dc}$. The density of germanium (near 300 °K) is 5.32 g/cm3 from which v_{Ge} ~ 13.65 cm^3/mol. From published results on the rate of volumetric expansion of germanium, η = 0.59 (Liang et al.).[86] Using these values, the stress-chemical potential coupling in this system is estimated to be $\frac{\partial \mu}{\partial \sigma} \approx 5.3\ KJ/mol.GPa$. The term $\frac{\partial \sigma}{\partial c}$ is the slope of stress versus concentration curve showed in Figure 3.1b and is approximately $M\eta$ at low lithium concentration where *M* is biaxial modulus. Tripuraneni and Nadimpalli [101] measured the biaxial modulus of lithiated Ge and for the low concentration of lithium the values is 45 GPa. Substituting all the values parameters, the ratio of the mechanical to chemical terms in Equation (3.7) at low Li concentration is approximately 5.6, suggesting a strong contribution from the stress, i.e., the variation in the $\widetilde{D}$ is due to combination of stress and concentration. This estimate is very close to the value of 11 estimated by Papakiriyoku et al.[102] for $Li_{1.3}Ge$ material. However, at the very high lithium concentration levels (i.e., as $c \rightarrow c_{max}$), the chemical enhancement factor will become larger along with mechanical contribution as the term $\frac{c_{max}}{c_{max}-c}$ increases rapidly at the end. This could be noticed from the sharp increase in $\widetilde{D}$ at the end of lithiation in Figure 3.6a.

Figure 3.6a shows that the nature of stress also influences the transport, i.e., $\widetilde{D}$ values obtained during lithiation (i.e., when the film was under compressive stress) are less than those obtained during delithiation (i.e., when the film was under tensile stress). For

example, the $\widetilde{D}$ value at x = 1.4 during delithiation (40 X 10^{-15} cm^2/s) is twice the value (20 x 10^{-15} cm^2/s) at the same Li concentration during lithiaton (x = 1.4), because in the former case the electrode is under tension with a stress value of 0.4 GPa whereas in the latter case it was under a compressive stress of -0.4 GPa. A similar effect of stress on transport was reported by Aziz et al. [103] where it was shown experimentally that the tensile stress enhanced the rate of solid-phase epitaxial-growth rate of crystalline Si from amorphous Si while compressive stress impeded the reaction. Some evidence of stress on lithiation was provided by Gu et al., [90]which showed that when a bent nanotube was reacted with Li, the regions under tensile stress lithiated relatively faster than those under compressive stress; their qualitative observation provides further support to the data presented in Figure 3.6a. This can be further understood through an activation energy based argument. For example, diffusion of a solute atom in a lattice can be described as a sequence of jumps from one interstitial lattice site to an adjacent site by surmounting the energy barrier caused by surrounding atoms. Haftabaradaran et al. [104] showed that a compressive stress increases this energy barrier (i.e., impedes diffusion) while tensile stress reduces the energy barrier (i.e., promotes diffusion). Atomic structure and associated changes in atomic arrangement could also contribute to the activation energy barrier; however, it is reasonable to assume that stress is the primary reason for the observed offset in $\widetilde{D}$ values presented in Figure 3.6a and not the atomic structure. This is because all the sputtered Ge films (which are amorphous to begin with) in the current study were cycled above 50 mV vs. Li/Li^+ which ensured that the film remained amorphous throughout the experiment; the continuously varying potential in Figure 3.1a supports this and agrees with earlier in situ XRD studies. [89] As a result, at a given Li concentration, one can expect a similar atomic

environment at any given location in the film irrespective of lithiation/delithiation process, ruling out the possibility; hence, proving further support to the argument that the stress is primarily contributing factor to the observed offset in $\widetilde{D}$ values at a given concentration in Figure 3.6.

In summary, the data presented here shows that the chemical diffusion coefficient $\widetilde{D}$ is a strong function of not only Li concentration but also electrode stresses. This is very important in the context of next generation high energy density anode materials, which are usually subjected to significant stresses during electrochemical cycling due to large volume expansion behavior; also, the observations are directly relevant to all solid-state batteries which are in general thin films with similar mechanical constraints as the Ge electrodes in this study. Therefore, ignoring the effect of stress on diffusion coefficient in battery models may lead to errors in estimated electrode stresses, electrode potentials, and lithiation/delithiation kinetics. Therefore, the multiphysics models that attempt to simulate the battery operation, for example, [69][99][105-106] should consider the effect of both Li concentration and electrode stresses on Li transport as per Figure 3.6. It should be noted that the $\widetilde{D}$ values presented here should be considered as first order estimates due to the assumptions mentioned above. Nonetheless, the data and the observations made in this study are crucial for electro-chemo-mechanics modeling of batteries and subsequent design/optimization of superior electrodes.

3.4 Conclusions

The data from PITT experiment was analyzed to obtain the chemical diffusion coefficient value. As expected, the $\widetilde{D}$ increases significantly with Li concentration both during lithiation and delithiation; for example, it increases from a value of 30 X 10^{-15} cm^2/s at x = 0.1 to a value greater than 150 X 10^{-15} at x > 3.1 for delithiation. In addition, the $\widetilde{D}$ values obtained during lithiation are at least two times smaller than those obtained from the delithiation process at any given lithium concentration with the difference increasing to as high as four times at higher Li concentration. It was demonstrated that the stress contribution to the transport processes is significant and the nature of stress (i.e., tension vs. compression) has significant effect on the Li transport. For example, the $\widetilde{D}$ value at x = 1.4 during delithiation (40 X 10^{-15} cm^2/s) is twice the value (20 x 10^{-15} cm^2/s) at the same Li concentration during lithiaton (x = 1.4), because in the former case the electrode is under tension with a stress value of 0.4 GPa whereas in the latter case it was under a compressive stress of -0.4 GPa. Hence, the data shows quantitatively that the tensile stress enhances transport while compressive stress impedes it. In summary, the data presented here show that the chemical diffusion coefficient $\widetilde{D}$ is a strong function of Li concentration as well as electrode stresses. This is a crucial data for electro-chemo-mechanics modeling of batteries and subsequent design of superior electrodes.

CHAPTER 4

STRUCTURAL CHANGES AND ASSOCIATED STRESS EVOLUTION ON GE ANODE AS NA-ION BATTERY ELECTRODE DURING SODIATION/DESODIATION CYCLING

4.1 Introduction to Na-Ion Battery

The recent push towards environmentally friendly energy production and gasoline-free transportation technologies has renewed the interest in developing advanced energy storage devices such as rechargeable batteries. Owing to an unparalleled volumetric and gravimetric energy densities among the available battery chemistries,[35][107] lithium-ion battery (LIB) has been the primary choice as energy storage device in portable electronics, electric vehicle, and grid-storage applications. However, projected widespread use of electric vehicles in the near future will increase the demand for Li and drives the cost higher, because lithium reserves are limited and located in the politically sensitive and geographically remote areas of the earth. As a result, efforts of developing viable and alternative batteries such as Al, Mg, and Na ion batteries have been increased recently. Among these options, the sodium-ion batteries (NIB) are gaining momentum to be the potential replacement of lithium-ion batteries, especially for grid-storage applications where low cost is the primary requirement. Sodium-ion batteries are cheaper due to the abundance of Na in the Earth's crust.[108-110] Further, Na does not react with Al, [23] which enables replacing costly Cu with Al as the current collector, another practical advantage that makes sodium-ion batteries significantly cheaper.

Since Na is chemically similar to Li in many aspects, and the fundamental principles of NIB and LIB are identical, much effort has been dedicated to identifying electrode materials that are structurally similar to those used in lithium-ion battery technology. [23][110-111] A significant success has been achieved with such an approach in finding positive electrode materials for sodium-ion battery; for example, layered type transition metal oxides and tunnel structured manganese oxides have shown to reversibly intercalate/deintercalate Na-ions successfully, resulting in stable capacities of more than 140 mAh/g for several hundred cycles. [35] However, a search for suitable anode material is still in progress. Graphite, widely used negative electrode in lithium-ion batteries, is not suitable for sodium-ion batteries as it inhibits the intercalation of Na atom.[112] On the other hand, the hard carbons have shown to react reversibly with Na producing a capacity of 300 mAh/g.[113] The other promising negative electrode materials for sodium-ion batteries are amorphous Ge (369 mAh/g),[114-115] Pb (485 mAh/g),[115-116] Sb (660 mAh/g),[115-117] and Sn (847 mAh/g).[117-118] Although these materials have comparable specific gravimetric capacities to those of Li-ion battery negative electrodes, they suffer from poor cyclic performance. [119-120] Among the available negative electrode material choices, Ge showed reasonable capacity retention; for example, Abel et al. [121] have showed that a nanocolumnar Ge retained 88% of the initial capacity for more than 100 cycles.

It has been shown in lithium-ion battery literature that volume expansion induced stresses dictate the long-term cyclic performance. For example, Si, Sn, and Ge expand almost 300% upon reacting with Li which induces a significant amount of stresses in these electrodes. Bucci et al., [12] Al-obedi et al.,[13] Nadimpalli et al., [14] Pharr et al.,[80] and

Soni et al.,[18] have experimentally showed that the magnitude of stresses in various electrode materials due to lithiation/delithiation cycling could reach as high as 1.5 GPa. These volume expansion induced stresses have been shown to cause extensive plastic deformation and fracture of electrodes resulting in rapid capacity fade. [19-21][123]It is also observed that the mechanical properties such as tensile modulus, Poisson's ratio, and yield stress vary with Li concentration, [11] [22] this continuous variation of properties throughout battery operation will affect its cyclic performance. Besides being the driving force for mechanical damage and capacity fade, stresses also affect the reaction kinetics, [85][87] and transport processes. [124] It is expected that the volume expansion induced stresses in sodium-ion battery electrodes will play a similar role and affect the cyclic performance of sodium-ion batteries. In fact, this effect could be amplified owing to the bigger size of Na-ion compared to that of Li-ion. Hence, quantifying stresses generated due to sodiation/desodiation reactions is important to understand the damage evolution in sodium-ion battery electrodes. This information is necessary for designing damage tolerant and high-performance electrode architectures for NIBs. Significant amount of work has been done on the electrochemical behavior of various sodium-ion battery electrodes, but, in spite of its importance, their mechanical behavior has not yet been characterized. The lack of experimental data on the mechanical characterization also hinders the development of multiphysics mathematical models for sodium-ion batteries.

Hence, the primary objective of this study is to measure the amount of volume expansion and the associated stresses in Ge electrodes during sodiation/desodiation reactions. To this end, sputter deposited Ge films on a double side polished (DSP) fused silica wafers were cycled electrochemically against Na foil

(counter/reference) electrode in a beaker cell; the electrodes in this half-cell configuration were separated by a microfiber filter to avoid short circuit. While the Ge film was cycled under galvanostatic conditions, the substrate curvature of DSP silica wafer was monitored using an optical technique to provide real-time stress measurements in the Ge thin film electrode. The volume expansion of Ge as a function of sodium concentration was obtained by measuring the thickness of multiple Ge thin film electrode samples that were sodiated/desodiated to different states of charge (SOC); all the experiments were conducted in an argon filled glove box. The film thickness changed irreversibly after the first cycle, i.e., the Ge film did not return to its original thickness after a full sodiation and desodiation cycle. It was observed that the steady state stress-capacity response of Ge film during sodiation/desodiation showed qualitatively similar behavior to that of lithiated Ge film, but the magnitude of stress differs significantly. It was interesting to see that the peak stress values of Na_xGe was lower than that of Li_xGe, in spite of significantly bigger Na-ion size compared to Li-ion. The reported volume expansion data and real-time stress measurements of sodiated Ge will serve as the foundation for developing mechanics-based models of sodium-ion battery electrodes and damage tolerant electrode design efforts.

4.2 Experimental Methods

4.2.1 Ge thin film electrode fabrication Ge thin films deposition was similar to the process explained in Chapter 2 experimental section. The XRD spectrum of an as deposited sample, shown in Figure 4.1, obtained by X-Ray Diffractometer (Bruker D8 Discover X-Ray Diffractometer, Bruker Corporation) confirms the amorphous nature of fabricated Ge

thin films. The peaks shown in the XRD pattern, an indication of crystallinity, belongs to Cu, but no peaks exists for Ge confirming its amorphous nature. [88]

4.2.2 Electrochemical Cell Assembly and Measurements The sodium-ion half cells were assembled and cycled at room temperature inside an argon-filled glove box (MBraun Inc., < 0.1 ppm O_2, < 0.1 ppm H_2O). The amorphous germanium (a-Ge) film as a working electrode, 1.3 mm thick sodium foil (prepared from Na cubes 99% trace metals basis, Sigma Aldrich) as a counter/reference electrode, and 1M sodium perchlorate ($NaClO_4$,>98% pure, Sigma Aldrich) in propylene carbonate (PC, 99.7% anhydrous, Sigma Aldrich) with 5 wt.% fluoroethylene carbonate additive (FEC, Sigma Aldrich) as an electrolyte were used to make electrochemical cells. A glass microfiber filter (pore size ~1 µm, Sigma Aldrich) was used as separator, which prevents any physical contact between electrodes, i.e., avoids short circuit.

The amorphous Ge films were sodiated and desodiated under galvanostatic (i.e., a constant current density of i = 1 µA/cm^2) conditions between 2 V and 0.001 V vs. Na/Na$^+$ using a Solartron 1470 E potentiostat; the stress and potential response of the Ge film was recorded simultaneously during this process. Scanning electron microscopic analysis was done on as-prepared and cycled samples. The cycled cells were dissembled, and the samples were rinsed with propylene carbonate for 10 min followed by 24 h of drying inside the glove box before conducting SEM analysis. The samples were carried in a sealed argon-filled container to transfer into the SEM chamber with minimum exposure ambient air.

4.2.3 Stress Measurements Using Multi Beam Optical (MOS) Setup The schematic of the multi-beam optical sensor (MOS) set up (k-Space Associates, Dexter, MI) which was used to monitor the curvature evolution of fused silica substrate during sodiation/desodiation cycling of Ge film is similar what has been used in Chapter 2.

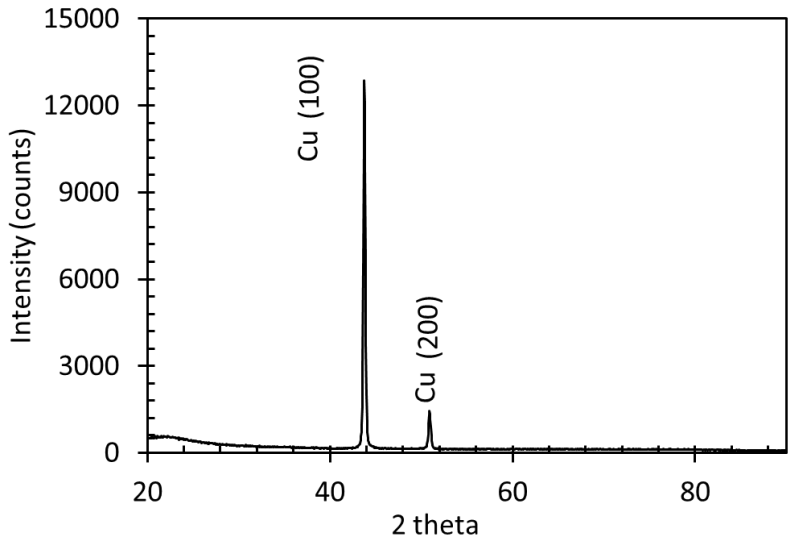

(c)

Figure 4.1 XRD pattern of the as deposited films on silica substrate conforming the amorphous nature of Ge film (i.e., no peaks for crystalline Ge).

The stresses in the Ge film are related to the substrate curvature by Stoney's equation,

$$\sigma = \sigma_r + \frac{E_s t_s^2 k}{6 t_f (1-\upsilon_s)} \tag{4.1}$$

where E_s is the Young's modulus, t_s the thickness, and υ_s the Poisson's ratio of the silica substrate. The parameter σ_r is residual stress in the as prepared Ge film (due to deposition process), and t_f is the thickness of the a-Ge film which will change continuously during sodiation/desodiation reaction. Based on the previous observations of Li-ion electrodes,[125] it is reasonable to assume that the volume expansion of Ge will be a linear

function of sodium concentration, i.e., the thickness evolution of Ge film as a function of capacity due to sodiation/desodiation is given as

$$t_f = t_f^0(1 + \beta z) \tag{4.2}$$

Here, t_f^0 is initial film thickness, z is state of charge (SOC) which changes between 0 and 1; z =1 corresponds to a fully sodiated state with a capacity of 369 mAh/g and a volumetric strain of β. The volumetric strain in Ge due to sodium reaction has not been measured experimentally before. Note from Equation (4.2) that the instantaneous film thickness t_f is required to determine the true stress in the film. Hence, volume expansion behavior of Ge due to sodiation/desodiation reaction was measured, the details of which are presented in the following section.

4.2.4 Volume Expansion Measurement of Ge due to Sodiation/Desodiation Reaction

A patterned Ge film as shown in Figure 4.2 was fabricated by a sequence of nano and microfabrication processes such as photolithography, e-beam evaporation, and lift-off (microposit remover) on a double side polished fused silica (thickness ~500 μm, length 25 mm, width 25 mm). The thickness of Ge, Ni, and Ti films was 30 nm, 75 nm, and 5 nm, respectively. The patterned Ge sample was then assembled in a half cell configuration, with Na foil (~1.3 mm thickness) as the reference/counter electrode and 1M sodium perchlorate ($NaClO_4$,>98% pure, Sigma Aldrich) in propylene carbonate (PC, 99.7% anhydrous, Sigma Aldrich) with 5 wt.% fluoroethylene carbonate additive (FEC, Sigma Aldrich) as the electrolyte.

Exposed silica substrate (shown in (Figure 4.2a) and (Figure 4.2b)), acts as a reference level to measure the thickness expansion/contraction of Ge thin film electrode during sodiation/desodiation reaction; note that the thickness of Ni and Ti does not change

as these films do not react with sodium. The patterned electrodes were cycled in a beaker cell configuration (similar to Figure 2.2a in Chapter 2) under galvanostatic conditions to different state of charge levels; specifically, three samples for after the completion of first sodiation process, three samples for the first cycle (one complete sodiation/desodiation), and three samples for the completion of second sodiation (one sodiation after 1^{st} cycle) were interrupted respectively for further AFM measurement. The interrupted cells were then dissembled, and samples were rinsed in propylene carbonate (PC) for 10 minutes followed by 24 h drying inside the glove box before carrying out the thickness measurements with the help of AFM.

The thickness measurements were carried out using an atomic force microscope (Icon, Bruker Corporation) which is sitting inside a glove compartment (Mbraun Inc, filled with Ar, <0.1 ppm O_2 and <0.1 ppm H_2O). Here, Figure 4.2b and 4.2c show the topology and thickness data of as prepared sample measured using AFM. In each cycled sample the thickness measurements were performed at multiple locations and an average of all these were taken as a representative measurement from a single sample. The SCANASYST-AIR (Bruker Corporation, spring constant 0.4 N/m) probe was used for the thickness measurement. The measurements were made in tapping mode.

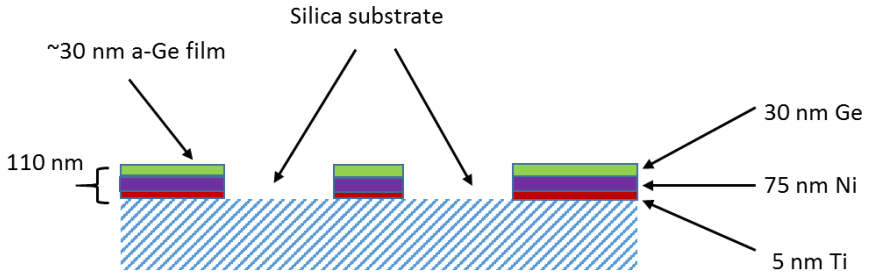

(a)

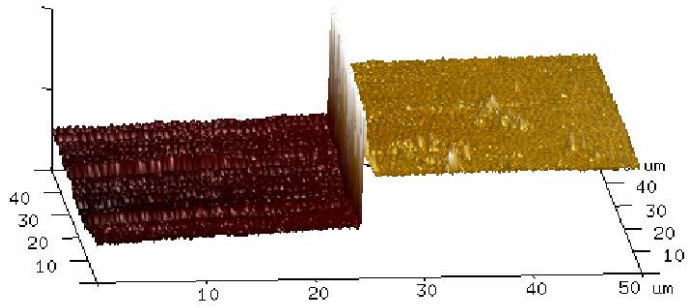

(b)

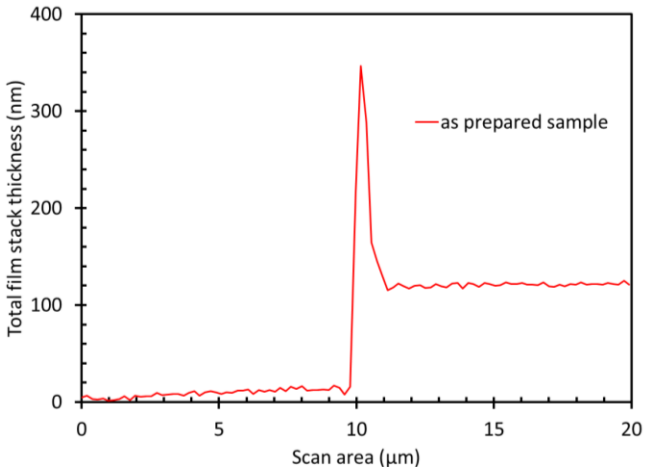

(c)

Figure 4.2 (a) Schematic of patterned electrode, designed for volume expansion study; (b) the scanned AFM image at a typical location of interest in the as prepared patterned sample; (c) the profile of patterned sample showing the 110 nm stack of films (~5 nm Ti, ~75 nm Ni, and ~30 nm Ge).

4.3 Results and Discussion

4.3.1 Potential Response of Ge Electrode during Sodiation/Desodiation Figure 4.3 shows the potential response of Ge film as a function of specific capacity and time, respectively.

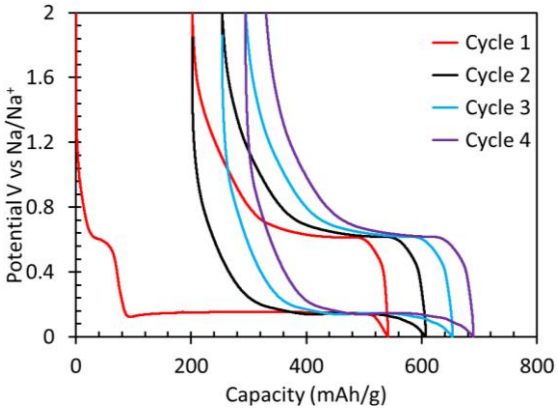

(a)

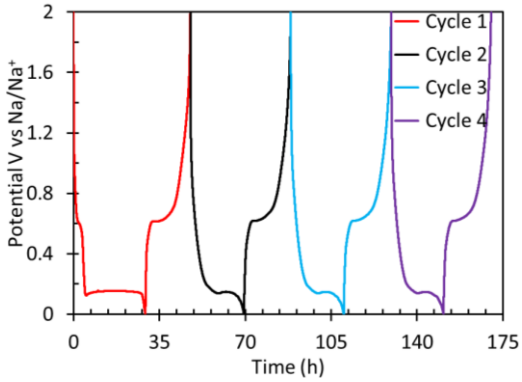

(b)

Figure 4.3 Potential response of Ge thin film anode as a function of (a) capacity and (b) time during sodiation/desodiation cycling at a constant current density of ~1 μA/cm^2 with C/20 rate.

The electrodes were cycled under a constant current density of 1 $\mu A/cm^2$ (which corresponds to C/20 rate). It can be noted that at the beginning of the first cycle, the potential of the cell drops sharply from an open-circuit value of 2 to 0.61 V *vs.* Na/Na^+ where it remains constant for a short period of time before it reaches to a voltage plateau of 0.14 V *vs.* Na/Na^+. The potential plateau at 0.14 V *vs.* Na/Na^+ corresponds to sodium insertion into Ge film. The potential remains constant at 0.14 V *vs.* Na/Na^+ until the end of sodiation and drops suddenly to the cut off value of 0.001 V *vs.* Na/Na^+ at 540 mAh/g. Upon desodiation, the potential rises sharply to 0.65 V *vs.* Na/Na^+ within a 40 mAh/g change in capacity and remains constant until the capacity decreases to 360 mAh/g, corresponding to sodium extraction from Ge film. After that, potential gradually rises to 2 V *vs.* Na/Na^+ at the end of desodiation process with a capacity of 200 mAh/g. The columbic efficiency in the first cycle was 63%, it increased to 78% in the second and to 81% in the fourth cycle. The short plateau of 0.61 V *vs.* Na/Na^+ that is present in the first cycle sodiation process but almost nonexistent in the rest of the cycles (Figure 3a and 3b) can be attributed to irreversible side reactions, which leads to the formation of a passivation layer called solid electrolyte interphase layer (SEI) layer. [88] Also, the Ge films with different thickness were cycled at different C rate and the potential responses were similar in every case.

The flat potential response such as at 0.14 V *vs.* Na/Na^+ during sodiation and at 0.65 V *vs.* Na/Na^+ during desodiation in (Figure 3), in general, it is an indication of a two-phase reaction in the electrodes, i.e., insertion reaction leads to formation of a phase that creates a sharp phase boundary separating two regions (or two equilibrium phases) with a sharp concentration across the phase boundary. This sharp phase boundary propagates into the

film during sodiation process until the entire film is turned to a single phase. For example, graphite,[39] Al[40] and, Sn[15][41] exhibit two-phase reactions leading to constant potential response during lithiation/delithiation process. In fact, it was reported by [14][42][43] that the sodiation of Sn also exhibits flat potentials indicating two-phase reactions similar to that occurs during lithiation process. It should be noted that the electrodes in most of these studies, Sn for example, are crystalline in nature and transform into crystalline intermetallic compounds during electrochemical cycling; lithiation of crystalline Si results in the formation of amorphous LixSi phase that propagates into the sample leading to a flat potential response. However, there is an interesting difference between these previous reports and the present study, i.e., the Ge thin film electrodes in the present study are amorphous in nature to start with, see Figure 4.1, yet a flat potential response was observed suggesting a two-phase reaction has occurred. This is interesting because lithiation of amorphous germanium or amorphous silicon does not produce a two-phase reaction and instead it leads to a solid solution of Li and Si or Li and Ge. Although not conclusive but under some special conditions Li et al., [127] did observed a similar two-phase reaction in amorphous Si (or a-Si), i.e., when a-Si was lithiated it formed a-Li_xSi and a clear phase boundary between a-LixSi and unreacted pristine a-Si, in further lithitation, the width of a-Li_xSi is increasing and finally it becomes a single phase when the entire electrode is fully lithiated. It is expected that similar kind of phenomena is occurring in the a-Ge film in Figure 4.3a.

According to Baggetto et al., [115] who carried out *in situ* X-ray diffraction measurements of sputter deposited amorphous Ge films similar to those fabricated in this

study, the amorphous Ge film remains amorphous Na_xGe film at the end of sodiation process.

4.3.2 Stress Response of Ge Thin Film Electrode during Sodiation/Desodiation Reaction

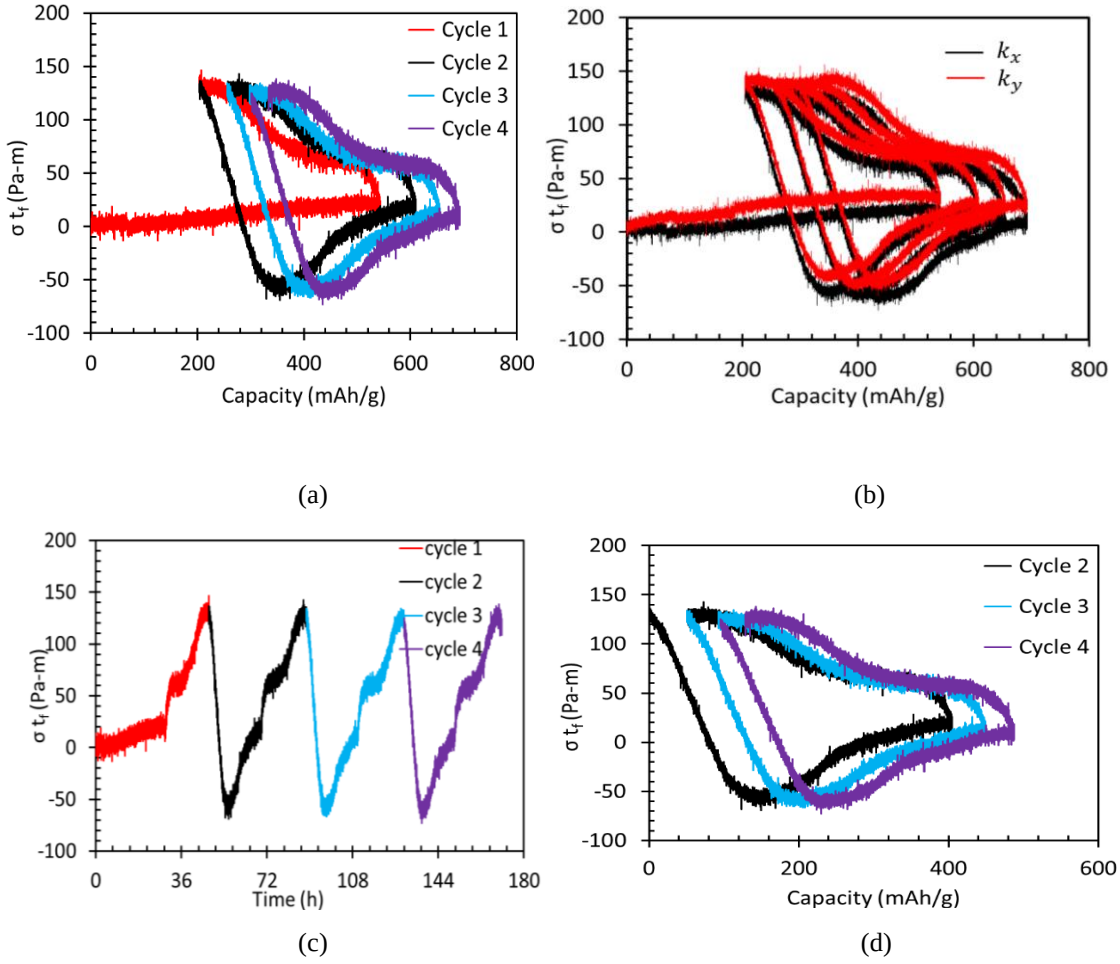

Figure 4.4 Real-time electro-chemo-mechanical behavior of Ge thin film anode during sodiation/desodiation cycling at constant current ~1 μA/cm^2 with C/20 rate (a) stress-thickness as a function of cell capacity (b) stress-thickness as a function of cell capacity measured in two different directions (orthogonal to each other) in same sample, (c) stress-thickness value (or substrate curvature) as a function cycled time, (d) stress-thickness as a function of cell capacity from 2nd cycle onwards.

The curvature of the film was measured before and after Ge film depositions which was used to calculate the residual stress of the film. The measured average residual stress was -0.24 GPa.

Figure 4.4a presents the variation of substrate curvature (proportional to stress-thickness value) as a function of specific capacity of Ge thin film during sodiation/desodiation reaction with the help of MOS (Multi Beam Optical Sensor) set up. The residual stresses in the a-Ge film were measured by recording substrate curvature changes before and after a-Ge film deposition with the help of MOS set up, which was -0.24 GPa. Generally, upon sodiation the Ge film expands in thickness direction which is direction normal to the plane of the silica substrate. Substrate does not allow to the in-plane expansion of the sodiated Ge film and film expands only in thickness direction (z direction) which results compressive stress. In general, substrate curvature changes with the sodium ion concentrations during electro-chemical cycling, however, the stresses during 1^{st} sodiation did not change much and apparently it looks like a flat line. Upon 1^{st} desodiation, Ge film is subjected to tensile stresses which is repeatable in subsequent desodiation cycles. In subsequent cycles, the stress peak reached to maximum value -65.53 Pa-m (compressive) during sodiation and maximum to 146.61 Pa-m (tensile) upon desodiation. This stress response is consistent with different fresh samples (at least 10 set of repeatable data), fabricated in different batches, which were cycled in the same condition. Here, Figure 4.4b indicates the stress-thickness as a function of cell capacity which was measured in two different directions (orthogonal to each other) of the sample. This result shows the isotropic volume expansion/contraction of the film during sodiation/desodiation. Figure 4.4c shows the stress-thickness as a function of time till 4^{th} cycle. Here, the peak stress magnitude till 4^{th} cycle is very much same which indicates the film did not crack till 4^{th}

cycle. Here, Figure 4.4d indicates the stress-thickness as a function of cell capacity from 2nd cycle to 4th cycle. In this figure, the 1st cycle was excluded to avoid any kind of stress contribution due to SEI formation. To understand the 1st sodiation stress response, more experiments were carried out at two different C rates i.e., in C/10 and C/30. Not only varying the C rate, the experiments were also carried out at different film thickness, i.e., on 30 nm and 100 nm as Ge thin film anode. However, the flat stress response was observed in all pristine samples in the 1st sodiation cycle. To measure the true stress (biaxial film stress), the exact volume expansion data is necessary. The volume expansion/contraction was measured on the samples (Figure 4.2a) *ex-situ* on the ~30 nm Ge anode with the help of AFM. The cycled samples potential response were similar to the earlier cycled 2 inch ~100 nm Ge electrode.

Figure 4.5a and 4.5b represent the images of as fabricated patterned electrode and electrode after 1st sodiation cycle, acquired by the Atomic Force Microscope. The height of the total film stack was 110 nm (where ~5 nm Ti, ~75 nm Ni, and ~30 nm Ge). The step-height was measured with respect to silica substrate which did not take part to the any kind of electrochemical reactions. Figure 4.5c represents the height of the Ge thin film at different sodium-ion concentration. Initial and final height of the Ge film were indicated by t_0 and t_f respectively. The volume expansion was measured on the patterned electrode at different states of charge (SOC's), such as end of 1st sodiation, end of 1st desodiation, and end of 2nd sodiation. The thickness measurements were performed on cycled film at least three different samples and two different locations of each sample. Upon full sodiation process the 30 nm Ge film became ~140.77 nm (standard deviation 7.02 nm, measured on multiple locations in three different samples) i.e., ~369% overall expansion. Upon

desodiation process, Ge film started contracting and it became 68.72 nm (standard deviation 11.53 nm, measured on multiple locations in three different samples), i.e., ~129% expansion respect to initial thickness. At the end of the 2nd sodiation process, the a-Ge film became ~142.07 nm (standard deviation 7.77 nm, measured on multiple locations in 3 different samples) i.e., ~107% volume expansion with respect to desodiated film (i.e, ~107% expansion with respect to the 1st desodiated film). The thickness of the sodiated and desodiated Ge film were measured at different patterned electrode location of the electrode, and the measured heights were almost same everywhere. This result shows that the expansion of Ge film is uniform throughout the electrode surface which in good agreement with the stress-thickness vs capacity plot (Figure 4b). The overall expansion of Ge film upon full sodiation is more than 300%, which is similar to the expansion of a-Ge nanowire-sodiation reported (300%) by Lu et al.[126] Here, Table 4.1 shows the sodiation/desodiation state and corresponding thickness of Ge thin film anode at different states of charge. In this study, the thickness of the thickness of solid electrolyte interphase (SEI) layer is neglected. It is also assumed that the volume expansion/contraction is in linear relation with Na ion concertation.

Table 4.1 Thickness Evolution on the Ge Thin Film Anode at Different States of Charge (SOC's).

Sample details	**Ge film thickness (nm)**
Pristine sample	~30
End of 1st sodiation	~140.77
End of 1st desodiation	~68.72
End of 2nd sodiation	~142.07

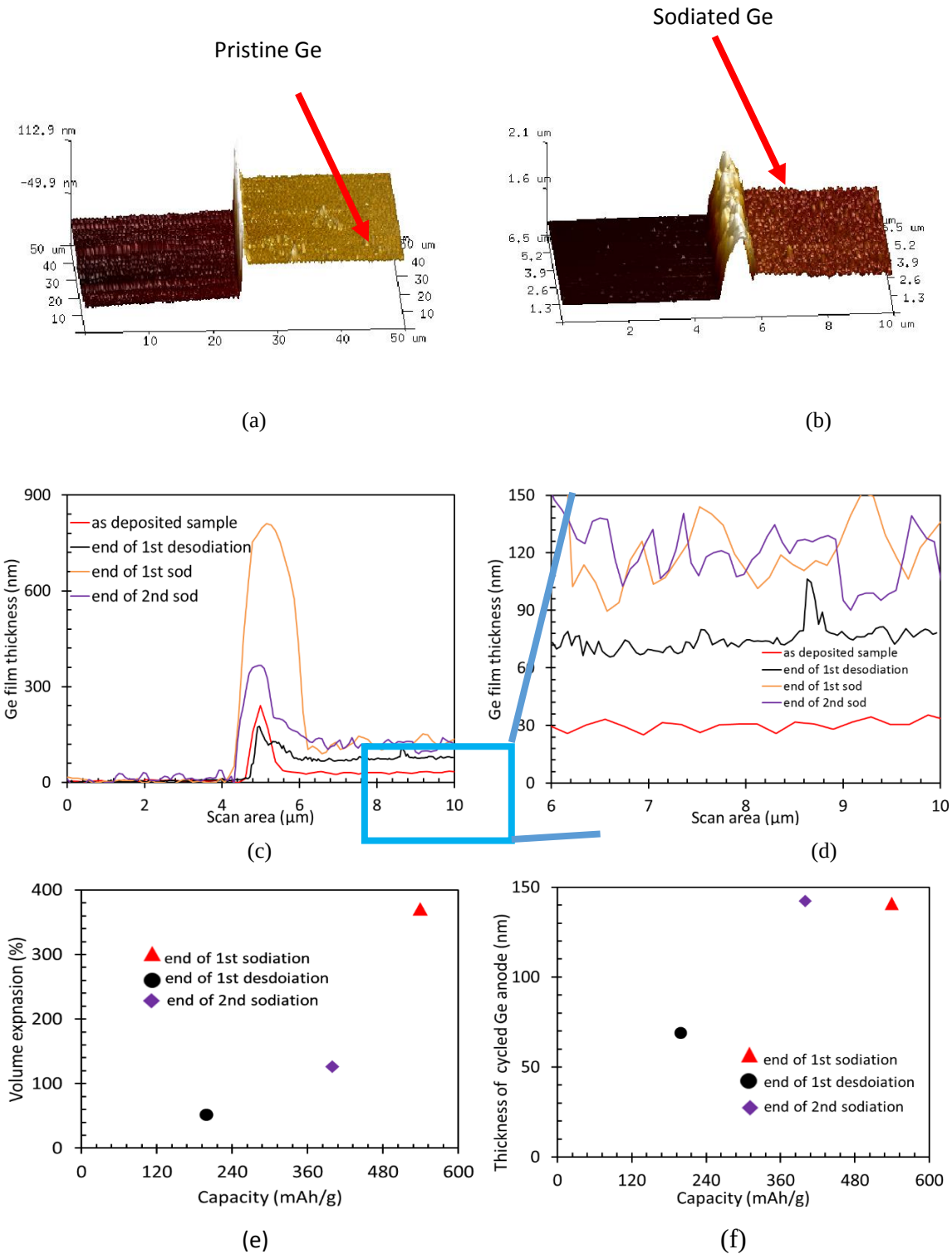

Figure 4.5 Profile of pristine and cycled electrode at different sodium ion concentration (a) AFM image of the as fabricated Ge anode, (b) AFM image at the end of 1st sodiation cycle, (c)-(d) Ge thickness of four samples at different sodium ion concentration (pristine sample, end of 1st sodiation, end of 1st desodiation, and end of 2nd soditaion), (e)-(f) volume expansion and thickness evolution of Ge thin film anode as a function of cell capacity.

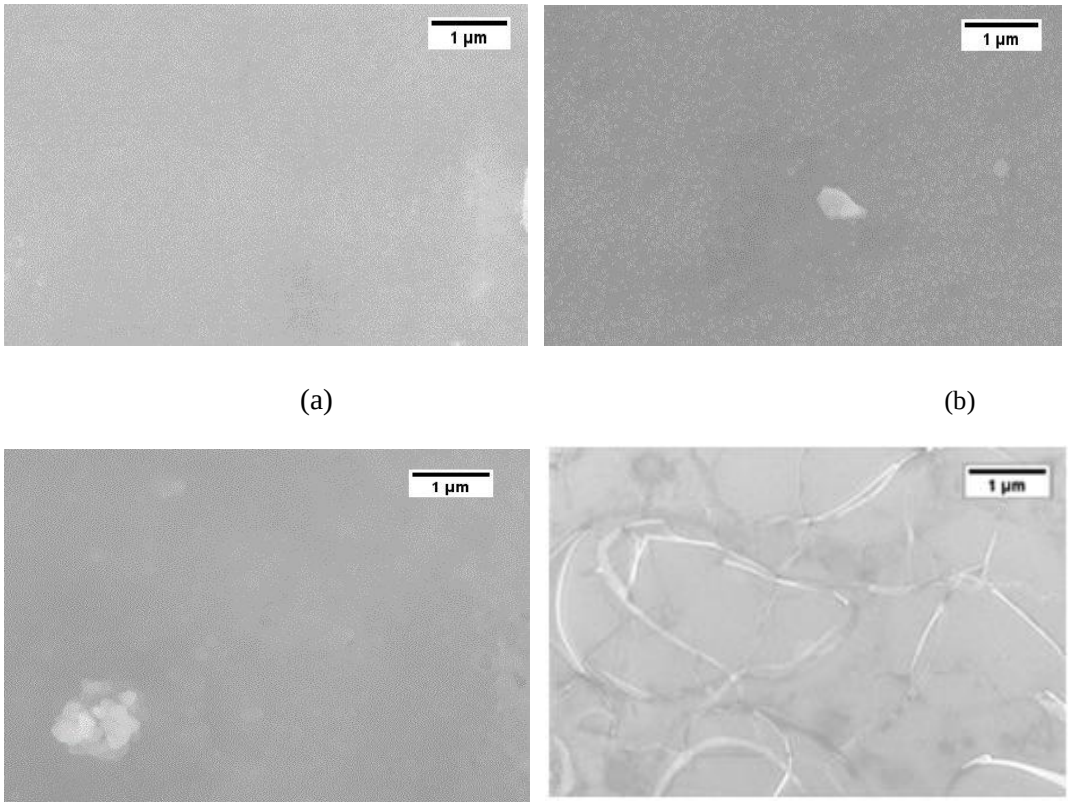

Figure 4.6 Surface morphology study of as deposited and cycled Ge thin film electrodes by SEM (scanning electron microscopy): (a) pristine a-Ge film, (b) Ge film after first sodiation, (c) Ge film after desodiation cycle, (d) Ge film after 5th cycle.

As it is discussed earlier, the 1st sodiation cycle in the a-Ge is a two phase reaction very much similar to a-Si with Li observed by Li et al., [127] A earlier discussed, a phase boundary is generated between the reacted Ge (NaxGe) and amorphous pristine Ge and this boundary is propagating though the ~100 nm Ge thin film electrode. Even though stress is flat in the 1st sodiation cycle, the volume expansion is similar to the obtained result at the end of 2nd sodiation cycle.

It is also mentioned in their study that lithiated crystalline Si converted to a-Si at the end of the end of delithiatiom through a two-phase reaction (crystalline-amorphous transition) and further lithiation the a-Si undergoes a single-phase reaction. It seems the

two-phase reaction is happening in 1st sodiation cycle similar to Li et al., [127] i.e., once the Ge is sodiated completely the stress behavior becomes repeatable/regular after that. Mitlin et al., [128] mentioned that NaGe system shows sluggish kinetics and poor cyclability which is a major drawback. To overcome that problem, they activated the Ge nanowire and Ge thin film by a lithiation/delithiation cycle, results in improvement in rate capability, stability etc. This phenomenon indicates that Ge thin film needs some kind of activation as sodium ion battery anode at initial cycling to overcome sluggish kinetics.

To investigate the 1st sodiation cycle, one more experiment was performed which is described here as forward-backward step experiment. The Figure 4.7a shows the outline of the conducted experiment, where the pristine a-Ge film subjected to sevens steps such as, step-1: sodiation till 4 hours, step-2: full desodiation, step-3: sodiation till 5 hours, step-4: full desodiation, step-5: full sodiation, step-6: full desodiation, step-7: full sodiation. Here, red boxes indicate the sodiation steps and black box indicates the desodiation steps. The galvanostataic sodiation/desodiation cycling was carried out with a current density 3 $\mu A/cm^2$ at ~C/10 rate. The film was sodiated partially for some time and then followed by full desodiation process. It is very interesting that the sodiation stress remains flat until it is sodiated once completely. Once it the Ge film is sodiated completely, then the stresses in subsequent cycle become regular and repeatable. This phenomenon is very much related with two-phase 1st sodiation reaction. Also, a complete desodiation might create some pores which makes Na ions easy to diffuse to the Ge film as it is discussed before.[44] One more interesting thing is observed here is that, a small magnitude of compressive stress is generated at the beginning of step-3 and step-5 (i.e., very beginning of the particular step). Upon 4-hour sodiation, though the sodiation stress is looks like a flat line however a small

amount of desodiation stress is generated which is prominent at the end of step-4. This small amount of desodiation stress magnitude is generated in step-2 and 4 because some part of the film is already activated upon sodiation process. The evolved stress-thickness response is similar to previously obtained result Figure 4a (~100 nm Ge film, cycled at ~1 μA/cm^2 with C/20 rate). It requires more experimental data to check the rate sensitivity of Ge towards Na, in this study rate sensitivity has not been studied.

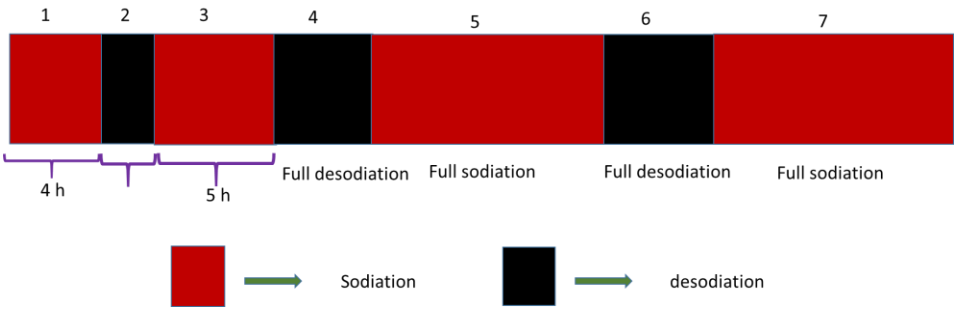

(a)

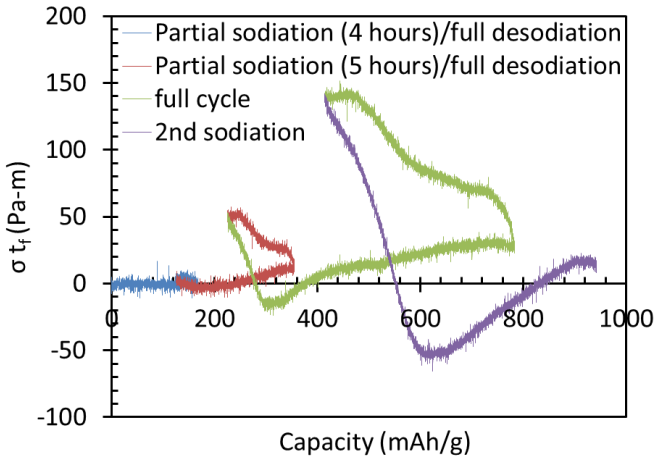

(b)

Figure 4.7 Schematic and results of conducted forward-backward galvanostatic step-experiments at C/10 rate in ~100 nm sputtered a-Ge film (a) outline for the conducted experiments (sodiation is indicated by red box, desodiation is indicated by black box), (b) stress thickness as a function of call capacity at different state of charge during electrochemical cycling.

Figure 4.8 represents the biaxial-stress (true stress) as a function of cell capacity at constant current ~1 μA/cm^2 with C/20 rate. The measured volume expansion data in earlier section is incorporated here to calculate the true stress on the thin film Ge electrode. Though the volume expansions were not measured in intermediate steps, it is assumed that the volume expansion is linear with the state of charge (SOC). In general, SEI is formed in early sodiation/desodiation cycle. To avoid the stress contribution due to the SEI formation, 1st sodiation/desodiation cycle is not shown in this plot.

$$t_f = t_f^0(1 + 1.076z) \tag{4.3}$$

t_f^0 is initial film thickness, z is state of charge (SOC) which changes between 0 and 1; z =1 indicates to a capacity of 369 mAh/g and a volumetric strain of 1.07.

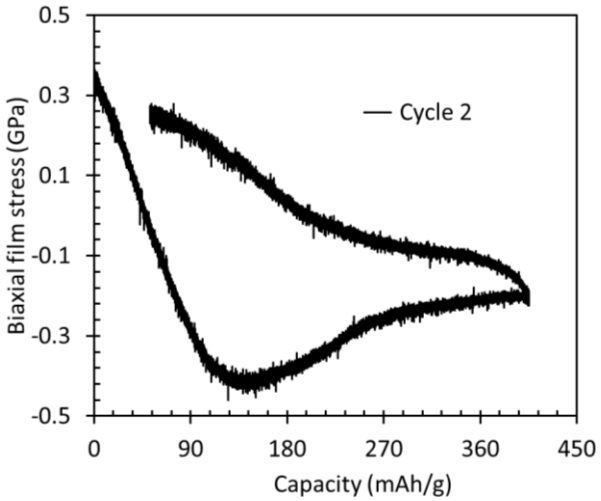

Figure 4.8 Biaxial-stress (true stress) as a function of cell capacity where the measured volume expansion data (from AFM samples) are incorporated here.

Upon initial sodiation, the biaxial stress is linear with sodium ion concentration which indicates the elastic response of the Ge anode. The stress response becomes non-linear at 105 mAh/g capacity, indicating the plastic flow of sodiated Ge. Upon sodiation, the stress peak reaches a peak value -0.43 GPa at 139 mAh/g and decrease to -0.21 GPa at 405 mAh/g. At the end of 2^{nd} desodiation process, the stress reaches to 0.25 GPa with a capacity 350 mAh/g.

4.4 Comparative study between Na-Ge and Li-Ge Figure 4.9a and 4.9b show the stress-thickness responses as a function of specific cell capacity between sodium-germanium (Na-Ge) and lithium-germanium (Li-Ge) system. The 1^{st} cycle data is ignored in both cases to avoid SEI layer formation. The maximum peak yield stress (stress-thickness) generated on Ge anode during lithiation is -70.87 Pa-m (compressive stress) and 189.64 Pa-m (tensile stress) upon delithaition. In case of sodiation the maximum peak stress (stress-thickness) in Ge film is -65.53 Pa-m (compressive) and 146.61 Pa-m (tensile) during desodiation. Having a bigger cationic radius, the peak yield stresses during charging and discharging in Na-Ge is less than Li-Ge system. The reason behind that, upon sodiation, Ge forms NaGe whereas Ge forms $Li_{15}Ge_{4,}$ i.e., Ge stores more Li ions compare to Na ions. It is very exciting, after forming NaGe, the peak stresses are lower in NaGe system which indicates probably NaGe is softer than Li_XGe.

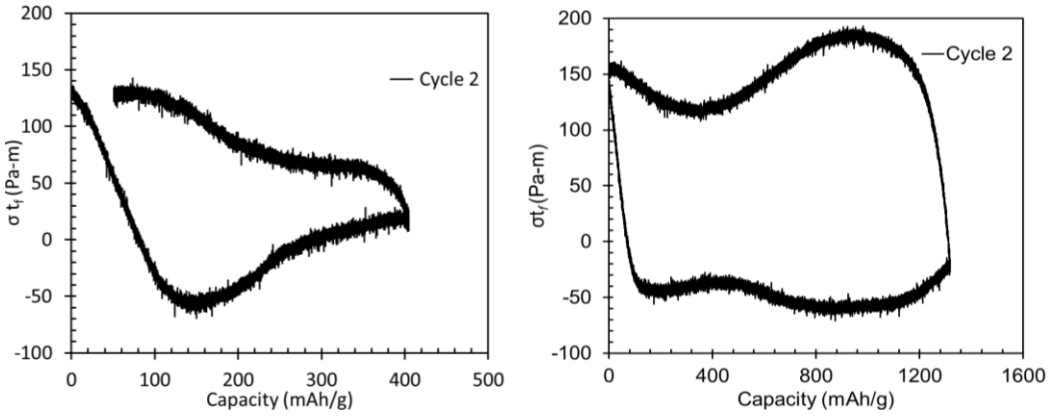

(a) (b)

Figure 4.9 A comparative study between Na-Ge and Li-Ge systems (a) stress thickness as a function of cell capacity on Ge anode in sodium ion battery, and (b) stress thickness as a function of cell capacity on Ge anode in lithium ion battery.

4.4 Conclusions

Here, we have explained the chemo-mechanical behavior of thin film Ge anode as Na ion battery electrode. The sample fabrication, experimental design, and characterization techniques have been described in detail. Real-time stress evolution study in a planar a-Ge thin film electrode will be a helpful to reveal many more exciting properties that depend on Na ion concentration during sodiation/desodiation process. Similar to lithiation process, sodiation of Ge leads to extensive plastic deformation of the electrode material during electrochemical cycling which has significant implications for the durability of electrodes. The experimental results show that during the sodiation/desodiation process, Ge film experienced a significant compressive/tensile stresses. The reported columbic efficiency in the first cycle was 64%, from 2^{nd} cycle onwards it started increasing and reached 80% at the end of 4^{th} cycle. The 36% capacity loss in the 1^{st} cycle is attributed to the SEI layer formation as well as some irreversible chemical reactions. The volume expansion/contraction of the sodiated/desodiated Ge film was studied with the help of in-situ AFM set up. The real-time biaxial film stress was measured based on the volume expansion results measured by *ex-situ* AFM. It is also explained that the peak stress during charging/discharging process is more on Li-Ge system compare to Na-Ge system. The stress response in 1^{st} sodiation cycle looks like a straight line approaching towards zero axis. The 1^{st} sodiation stress is completely different from subsequent cycles. The forward-backward experiment performed in the 1^{st} sodiation cycle explains, the film will not experience any significant stress untill the entire film is sodiated once. The SEM analysis shows the crack after 5^{th} cycle. Also, volume expansion measurement techniques will be helpful to measure on many more future electrode. Distinctly different mechanics and

electrochemical phenomenon were observed in Na-Ge system which will be helpful to reveal more exciting phenomena in Na-ion battery electrode.

CHAPTER 5

CONCLUSIONS AND FUTURE WORK

5.1 Conclusions

5.1.1 Chemo-Mechanical Behavior of SiO_2 Thin Film during Electrochemical Cycling

Real-time stress evolution in planar SiO_2 thin film electrodes were measured while cycling against Li foil counter/reference electrodes under galvanostatic lithiation/delithiation cycling. It was observed that upon lithiation the SiO_2 film undergoes compressive stress which increases linearly with Li concentration, below 70 mAh/g capacity and 0.4 GPa of stress, possibly representing a linear elastic response of the film. Upon further lithiation the electrode undergoes extensive plastic deformation with a peak compressive stress of 3.1 GPa at 450 mAh/g and thereafter decreases to 2.4 GPa at 756 mAh/g at the end of lithiation. Upon delithiation the stress quickly changes towards tensile direction and reaches a peak value of approximately 0.7 GPa. The first-cycle coulombic efficiency of the film was 78% which increases to 99% in the second cycle; in addition, potential and stress response of the film in the first lithiation process was significantly different from the subsequent cycles. This behavior along with the large first cycle loss was attributed to SEI formation and irreversible chemical reactions between SiO_2 and Li. Further, SEM analysis of the sample showed that the film was intact in the first cycle but started cracking after that. This premature cracking of SiO_2 in this study, as opposed to the coatings in earlier reports, which cycled without cracking for several hundred cycles, was attributed to relatively thick films in the current study, which tend to have a larger crack-driving force.

5.1.2 Effect of Stress on Transport Phenomena

To understand and quantify the effect of stresses on the chemical diffusion coefficient of Li, germanium was used as a model high energy density electrode. The sputter deposited Ge thin films were assembled in a half-cell configuration with a lithium foil as a reference/counter electrode. The electrodes were subjected to series of GITT and PITT protocols to measure the chemical diffusion coefficient as a function of Li concentration while simultaneously measuring the stresses in the electrodes using substrate curvature technique. To minimize the variation of stress, the titration steps were conducted when the electrode undergoes plastic deformation. In spite of this, a marginal change in stress (a change of ~60–90 MPa) was observed within a given titration step during a PITT experiment, which is due to the strain-rate sensitivity of electrode. A highly rate sensitive (rateinsensitive) material compared to Li_xGe would have resulted in more (less) than 90 MPa of stress change in a single titration step if subjected to the exact loading history. In contrast, the variation of stresses within a single titration step during GITT experiment was significant, i.e., 0.5 GPa, and is too big to be ignored in the analysis for evaluating diffusion coefficient. Hence, for electrode materials such as Ge, and other similar large volume change materials (Si, Sn, Al, and their alloys), the stress changes in a GITT experiment may be significant.

5.1.3 Real-time stress measurement on –ion battery anode

Here, we have explained the stress response of Ge electrodes in Na ion batteries. Real-time stress evolution in a planar a-Ge thin film electrode was measured during sodiation/desodiation cycling. Similar to lithiation, sodiation of Ge also leads to extensive plastic deformation during electrochemical cycling which has significant implications for

the durability of electrodes. The experimental results show that during the sodiation/desodiation process, Ge film experienced significant compressive/tensile stresses. At the end of the 1st desodiation process, the stress reached to 0.45 GPa which was gradually decreasing with subsequent desdoaition cycles. The reported columbic efficiency in the first cycle was 64%; from 2nd cycle onwards it started increasing and reached 80% at the end of 4th cycle. The 36% capacity loss in the 1st cycle is attributed to the SEI layer formation as well as some irreversible chemical reactions. The volume expansion/contraction of the sodiated/desodiated Ge film was studied with thr help of in-situ AFM set up. The expansion is in good agreement with the reported literature. SEM analysis shows the initiation of crack after 5th desodiation cycle though the exact time of cracking is not recorded here. Na-Ge system is not potentially favourable like Li-Ge system but the maginitude of evolved stresses is much lower. Thereby, Ge anode shows more mechanical stability to be used as a NIB anode. In summary, a lot of research work is going on to develop the electrochemical performance, but our real-time electrocehmistery-stress resposne along with volume expansion and phase analysis study will enlight to design better damage tolerant future anode for sodium-ion battery.

5.2 Future Work

- The Ge thickness expansion measurements in Chapter 4 did not take into account the formation of solid electrolyte interphase layer (SEI) which forms during sodiation/desodiation cycling. The SEI layer formation needs to be accounted for accurate measurement whichwill help in determining the accurate volume expansion of the anode material. Also, in-situ XRD during sodiation/desodiation process will be helpful to understand more about the possible phase change related phenomenon that may have contributed to flat stress response in 1st sodiation cycle.

- The Li diffusion coefficient was successfully measured in Ge thin film electrode. It would be interesting to measure the Na diffusivity in Ge with the same methods.

- Nanoporous electrodes show better cyclibility and capacity retention as Li and Na-ion battery anode. However, their mechanical properties have not been measured yet. It is expected that the magnitude of stress will be less in nanoporous electrode compared to its solid counterpart. This nanoporous electrode will be helpful for designing damage tolerant electrode architecture.

BIBLIOGRAPHY

[1] C. K. Chan, H. Peng, G. Liu, K. McIlwrath, X. F. Zhang, R. A. Huggins, and Y. Cui, "High-performance lithium battery anodes using silicon nanowires," *Nature Nanotechnology*, vol. 3, no. 1, pp. 31–35, 2008.

[2] N. Nitta and G. Yushin, "High-capacity anode materials for lithium-ion batteries: Choice of elements and structures for active particles," *Particle and Particle Systems Characterization*, vol. 31, no. 3, pp. 317–336, 2014.

[3] S. C. Jung, H. J. Kim, Y. J. Kang, and Y. K. Han, "Advantages of Ge anode for Na-ion batteries: Ge vs. Si and Sn," *Journal of Alloys and Compounds*, vol. 688, pp. 158–163, 2016.

[4] J. Li, F. Yang, X. Xiao, M. W. Verbrugge, and Y. Cheng, "Potentiostatic intermittent titration technique (PITT) for spherical particles with finite interfacial kinetics," *Electrochimica Acta*, vol. 75, pp. 56–61, 2012.

[5] Y. Zhu and C. Wang, "Galvanostatic intermittent titration technique for phase-transformation electrodes," *Journal of Physical Chemistry C*, vol. 114, no. 6, pp. 2830–2841, 2010.

[6] M. D. Levi, R. Demadrille, A. Pron, M. A. Vorotyntsev, and Y. Gofer, "Application of a novel refinement method for accurate determination of chemical diffusion coefficients in electroactive materials by potential step technique," *Journal of The Electrochemical Society*, vol. 152, no. 2, pp. 61–67, 2005.

[7] N. Ding, J. Xu, Y. X. Yao, G. Wegner, X. Fang, C. H. Chen, and I. Lieberwirth, "Determination of the diffusion coefficient of lithium ions in nano-Si," *Solid State Ionics*, vol. 180, no. 2–3, pp. 222–225, Mar. 2009.

[8] F. Varsano, F. Decker, E. Masetti, and F. Croce, "Lithium diffusion in cerium – vanadium mixed oxide thin films : a systematic study," *Electrochimica Acta*, vol. 46, pp. 2069–2075, 2001.

[9] H. Wu and Y. Cui, "Designing nanostructured Si anodes for high energy lithium ion batteries," *Nano Today*, vol. 7, no. 5, pp. 414–429, 2012.

[10] B. A. Boukamp, "All-solid lithium electrodes with mixed-conductor matrix," *Journal of The Electrochemical Society*, vol. 128, no. 4, p. 725, 1981.

[11] V. A. Sethuraman, M. J. Chon, M. Shimshak, V. Srinivasan, and P. R. Guduru, "In situ measurements of stress evolution in silicon thin films during electrochemical lithiation and delithiation," *Journal of Power Sources*, vol. 195, no. 15, pp. 5062–5066, 2010.

[12] G. Bucci, S. P. V Nadimpalli, V. A. Sethuraman, A. F. Bower, and P. R. Guduru, "Measurement and modeling of the mechanical and electrochemical response of amorphous Si thin film electrodes during cyclic lithiation," *Journal of the Mechanics and Physics of Solids*, vol. 62, no. 1, pp. 276–294, 2014.

[13] A. Al-Obeidi, D. Kramer, C. V. Thompson, and R. Monig, "Mechanical stresses and morphology evolution in germanium thin film electrodes during lithiation and delithiation," *Journal of Power Sources*, vol. 297, pp. 472–480, 2015.

[14] S. P. V Nadimpalli, R. Tripuraneni, and V. A. Sethuraman, "Real-time stress measurements in germanium thin film electrodes during electrochemical lithiation / delithiation cycling," *Journal of The Electrochemical Society*, vol. 162, no. 14, pp. 2840–2846, 2015.

[15] A. Ostadhossein, E. D. Cubuk, G. A. Tritsaris, E. Kaxiras, S. Zhang, and A. C. T. van Duin, "Stress effects on the initial lithiation of crystalline silicon nanowires: reactive molecular dynamics simulations using ReaxFF," *Physical Chemistry Chemical Physics*, vol. 17, no. 5, pp. 3832–3840, 2015.

[16] N. Liu, Z. Lu, J. Zhao, M. T. McDowell, H.-W. Lee, W. Zhao, and Y. Cui, "A pomegranate-inspired nanoscale design for large-volume-change lithium battery anodes," *Nature Nanotechnology*, vol. 9, no. 3, pp. 187–192, 2014.

[17] M. Pharr, K. Zhao, X. Wang, Z. Suo, and J. J. Vlassak, "Kinetics of initial lithiation of crystalline silicon electrodes of lithium-ion batteries," *Nano Letters*, vol. 12, no. 9, pp. 5039–5047, 2012.

[18] S. K. Soni, B. W. Sheldon, X. Xiao, and A. Tokranov, "Thickness effects on the lithiation of amorphous silicon thin films," *Scripta Materialia*, vol. 64, no. 4, pp. 307–310, 2011.

[19] J. R. Szczech and S. Jin, "Nanostructured silicon for high capacity lithium battery anodes," *Energy and Environmental Science*, vol. 4, no. 1, pp. 56–72, 2011.

[20] J. O. Besenhard, J. Yang, and M. Winter, "Will advanced lithium-alloy anodes have a chance in lithium-ion batteries?," *Journal of Power Sources*, vol. 68, no. 1, pp. 87–90, 1997.

[21] L. Y. Beaulieu, K. W. Eberman, R. L. Turner, L. J. Krause, and J. R. Dahn, "Colossal reversible volume changes in lithium alloys," *Electrochemical and Solid-State Letters*, vol. 4, no. 9, p. A137, 2001.

[22] V. B. Shenoy, P. Johari, and Y. Qi, "Elastic softening of amorphous and crystalline Li – Si Phases with increasing Li concentration : A first-principles study," *Journal of Power Sources*, vol. 195, no. 19, pp. 6825–6830, 2010.

[23] J.-Y. Hwang, S.-T. Myung, and Y.-K. Sun, "Sodium-ion batteries: present and future," *Chemical Society Reviews*, vol. 46, no. 12, pp. 3529–3614, 2017.

[24] W. Zhang, Y. Liu, and Z. Guo, "Approaching high-performance potassium-ion batteries via advanced design strategies and engineering," *Science Advances*, Vol 5, pp. 1–14, 2019.

[25] P. Novak, R. Imhof, and O. Hass, "Magnesium insertion electrodes for rechargeablenonaqueous batteries – a competitive alternative tolithium?," *Electrochemica Acta*, vol. 45, pp. 351–367, 1999.

[26] A. Ponrouch, C. Frontera, F. Bardé, and M. R. Palacín, "Towards a calcium-based rechargeable battery," *Nature Materials*, vol. 15, no. October 2015, pp. 1–5, 2016.

[27] S. Engelke, "Current and future sodium-ion battery research," *Storage4*, vol. 1, no. 1, pp. 1–7, 2013.

[28] H. Zhu, Z. Jia, Y. Chen, N. Weadock, J. Wan, O. Vaaland, X. Han, T. Li, and L. Hu, "Tin anode for sodium-ion batteries using natural wood fiber as a mechanical buffer and electrolyte reservoir," *Nano Letters*, vol. 13, no. 7, pp. 3093–3100, 2013.

[29] M. Gu, A. Kushima, Y. Shao, J.-G. Zhang, J. Liu, N. D. Browning, J. Li, and C. Wang, "Probing the failure mechanism of SnO_2 nanowires for sodium-ion batteries," *Nano Letters*, vol. 13, no. 11, pp. 5203–5211, Nov. 2013.

[30] W.-S. Chang, C.-M. Park, J.-H. Kim, Y.-U. Kim, G. Jeong, and H.-J. Sohn, "Quartz (SiO_2): a new energy storage anode material for Li-ion batteries," *Energy & Environmental Science*, vol. 5, no. 5, p. 6895, 2012.

[31] R. Ruffo, S. S. Hong, C. K. Chan, R. A. Huggins, and Y. Cui, "Impedance analysis of silicon nanowire lithium ion battery anodes," *The Journal of Physical Chemistry C*, pp. 11390–11398, 2009.

[32] P. P. Prosini, M. Lisi, D. Zane, and M. Pasquali, "Determination of the chemical diffusion coefficient of lithium in LiFePO4," *Solid State Ionics*, vol. 148, no. 1–2, pp. 45–51, 2002.

[33] C. J. Wen, B. A. Boukamp, and R. A. Huggins, "Thermodynamic and mass transport properties of ' LiAl ,'" *Journal of The Electrochemical Society*, vol. 126, no. 12, pp. 2258–2266, 1979.

[34] W. Weppner, "Determination of the kinetic parameters of mixed-conducting electrodes and application to the system Li3Sb," *Journal of The Electrochemical Society*, vol. 124, no. 10, pp. 1569–1578, 1977.

[35] B. L. Ellis and L. F. Nazar, "Sodium and sodium-ion energy storage batteries," *Current Opinion in Solid State and Materials Science*, vol. 16, no. 4, pp. 168–177, Aug. 2012.

[36] A. F. Bower, P. R. Guduru, and V. A. Sethuraman, "A finite strain model of stress, diffusion, plastic flow, and electrochemical reactions in a lithium-ion half-cell," *Journal of the Mechanics and Physics of Solids*, vol. 59, no. 4, pp. 804–828, 2011.

[37] J. Christensen and J. Newman, "Stress generation and fracture in lithium insertion materials," *Journal of Solid State Electrochemistry*, vol. 10, no. 5, pp. 293–319, 2006.

[38] L. Anand, "A Cahn-Hilliard-type theory for species diffusion coupled with large elastic-plastic deformations," *Journal of the Mechanics and Physics of Solids*, vol. 60, no. 12, pp. 1983–2002, 2012.

[39] U. Kasavajjula, C. Wang, and A. J. Appleby, "Nano- and bulk-silicon-based insertion anodes for lithium-ion secondary cells," *Journal of Power Sources*, vol. 163, no. 2, pp. 1003–1039, 2007.

[40] L. Y. Beaulieu, T. D. Hatchard, A. Bonakdarpour, M. D. Fleischauer, and J. R. Dahn, "Reaction of Li with alloy thin films studied by in situ AFM," *Journal of The Electrochemical Society*, vol. 150, no. 11, p. A1457, 2003.

[41] D. Aurbach, "Review of selected electrode-solution interactions which determine the performance of Li and Li ion batteries," *Journal of Power Sources*, vol. 89, no. 2, pp. 206–218, 2000.

[42] D. Aurbach, M. Moshkovich, Y. Cohen, and A. Schechter, "Study of surface film formation on noble-metal electrodes in alkyl carbonates/Li salt solutions, using simultaneous in situ AFM, EQCM, FTIR, and EIS," *Langmuir*, vol. 15, no. 8, pp. 2947–2960, 1999.

[43] E. Peled, "The Electrochemical Behavior of Alkali and Alkaline Earth Metals in Nonaqueous Battery Systems—The solid electrolyte interphase model," *Journal of The Electrochemical Society*, vol. 126, no. 12, p. 2047, 1979.

[44] J. O. Besenhard, M. Winter, J. Yang, and W. Biberacher, "Filming mechanism of lithium-carbon anodes in organic and inorganic electrolytes," *Journal of Power Sources*, vol. 54, no. 2, pp. 228–231, 1995.

[45] S. P. V Nadimpalli, V. A. Sethuraman, S. Dalavi, B. Lucht, M. J. Chon, V. B. Shenoy, and P. R. Guduru, "Quantifying capacity loss due to solid-electrolyte-interphase layer formation on silicon negative electrodes in lithium-ion batteries," *Journal of Power Sources*, vol. 215, pp. 145–151, 2012.

[46] R. Kostecki and F. McLarnon, "Microprobe study of the effect of Li intercalation on the structure of graphite," *Journal of Power Sources*, vol. 119–121, pp. 550–554, 2003.

[47] J. Vetter, P. Novak, M. . Wagner, C. Veit, K.-C. Moiller, J. O. Besenhard, M. Winter, M. Wohlfahrt-Mehrens, C. Vogler, and A. Hammouche, "Ageing mechanisms in lithium-ion batteries," *Journal of Power Sources*, vol. 147, pp. 269–281, 2005.

[48] Y. M. Lee, J. Y. Lee, H.-T. Shim, J. K. Lee, and J.-K. Park, "SEI layer formation on amorphous Si thin electrode during precycling," *Journal of The Electrochemical Society*, vol. 154, no. 6, p. A515, 2007.

[49] M. T. McDowell, S. W. Lee, I. Ryu, H. Wu, W. D. Nix, J. W. Choi, and Y. Cui, "Novel size and surface oxide effects in silicon nanowires as lithium battery anodes," *Nano Letters*, vol. 11, no. 9, pp. 4018–4025, 2011.

[50] H. Wu, G. Chan, J. W. Choi, I. Ryu, Y. Yao, M. T. Mcdowell, S. W. Lee, A. Jackson, Y. Yang, L. Hu, and Y. Cui, "Stable cycling of double-walled silicon nanotube battery anodes through solid-electrolyte interphase control," *Nature Nanotechnology*, vol. 7, no. 5, pp. 310–315, 2012.

[51] H. Wu, G. Yu, L. Pan, N. Liu, M. T. Mcdowell, Z. Bao, and Y. Cui, "Conformally coat silicon nanoparticles," *Nature Communications*, vol. 4, pp. 1943–1946, 2013.

[52] Y. Zhang, Y. Li, Z. Wang, and K. Zhao, "Lithiation of SiO_2 in Li-Ion batteries: in situ transmission electron microscopy experiments and theoretical studies," *Nano letters*, vol. 14, no. 12, pp. 7161–7170, 2014.

[53] S. Choi, D. S. Jung, and J. W. Choi, "Scalable fracture-free SiOC glass coating for robust silicon nanoparticle anodes in lithium secondary batteries," *Nano Letters*, vol 14, no. 12, 2014.

[54] Q. Sun, B. Zhang, and Z. W. Fu, "Lithium electrochemistry of SiO2 thin film electrode for lithium-ion batteries," *Applied Surface Science*, vol. 254, no. 13, pp. 3774–3779, 2008.

[55] M. Miyachi, H. Yamamoto, H. Kawai, T. Ohta, and M. Shirakata, "Analysis of SiO anodes for lithium-ion batteries," *Journal of The Electrochemical Society*, vol. 152, no. 10, p. A2089, 2005.

[56] Z. Favors, W. Wang, H. H. Bay, A. George, M. Ozkan, and C. S. Ozkan, "Stable cycling of SiO_2 nanotubes as high-performance anodes for lithium-ion batteries," *Scientific Reports*, vol. 4, pp. 1–7, 2014.

[57] B. Guo, J. Shu, Z. Wang, H. Yang, L. Shi, Y. Liu, and L. Chen, "Electrochemical reduction of nano-SiO2 in hard carbon as anode material for lithium ion batteries," *Electrochemistry Communications*, vol. 10, no. 12, pp. 1876–1878, 2008.

[58] N. Yan, F. Wang, H. Zhong, Y. Li, Y. Wang, L. Hu, and Q. Chen, "Hollow porous SiO2 nanocubes towards high-performance anodes for lithium-ion batteries," *Scientific Reports*, vol. 3, no. 1, p. 1568, 2013.

[59] B. Philippe, R. Dedryvere, M. Gorgoi, H. Rensmo, D. Gonbeau, and K. Edstrom, "Improved performance of nano-silicon electrodes using the salt LiFSI – A photoelectron spectroscopy study," *Journal of the American Chemical Society*, p. 130613104807005, 2013.

[60] K. Zhao, W. L. Wang, J. Gregoire, M. Pharr, Z. Suo, J. J. Vlassak, and E. Kaxiras, "Lithium-assisted plastic deformation of silicon electrodes in lithium-ion batteries: a first-principles theoretical study," *Nano Letters*, vol 11, no. 7, pp. 2962–2967, 2011.

[61] S. T. Boles, A. Sedlmayr, O. Kraft, and R. Mönig, "Battery applications in situ cycling and mechanical testing of silicon nanowire anodes for lithium-ion battery applications," *Applied Physics Letters*, vol. 100, no. 243901, pp. 3–7, 2012.

[62] J. Sheth, N. K. Karan, D. P. Abraham, C. C. Nguyen, B. L. Lucht, B. W. Sheldon, and P. R. Guduru, "In situ stress evolution in $Li_{1+x}Mn_2O_4$ thin films during electrochemical cycling in Li-ion cells," *Journal of The Electrochemical Society*, vol. 126, no. 13, pp. 2524–2530, 2016.

[63] J. Tu, Y. Yuan, P. Zhan, H. Jiao, X. Wang, H. Zhu, and S. Jiao, "Straightforward approach toward SiO_2 nanospheres and their superior lithium storage performance," *The Journal of Physical Chemistry C*, vol. 118, pp. 7357–7362, 2014.

[64] W. N. S. Jr, J. Pulskamp, and D. S. Gianola, "Strain measurements of silicon dioxide microspecimens by digital imaging processing," *Experimental Mechancis* vol. 47, no. 5, pp. 649–658, 2007.

[65] M. D. Levi and D. Aurbach, "Potentiostatic and galvanostatic intermittent titration techniques," *Characterization of Materials*, pp. 1-21, 2012.

[66] N. J. Dudney, W. C. West, and J. Nanda, *Handbook of solid state batteries,Second Edition*, vol. 6, no. Second Edistion. World Scientific Publishing Co. Pte. Ltd., 2016.

[67] M. Doyle, T. F. Fuller, and J. Newman, "Modeling of galvanostatic charge and discharge of the lithium / polymer / insertion cell," *Journal of the Electrochemical society*, vol. 140, no. 6, pp. 1526–1533, 1993.

[68] L. Cai and R. E. White, "Reduction of model order based on proper orthogonal decomposition for lithium-ion battery simulations," *Journal of The Electrochemical Society*, vol. 156, no. 3, pp. 154–161, 2009.

[69] C. V. Di Leo, E. Rejovitzky, and L. Anand, "A Cahn – Hilliard-type phase-field theory for species diffusion coupled with large elastic deformations : Application to phase-separating Li-ion electrode materials," *Journal of the Mechanics and Physics of Solids*, vol. 70, pp. 1–29, 2014.

[70] W. Weppner and R. A. Huggins, "Determination of the kinetic parameters of mixed-conducting electrodes and application to the system Li_3Sb," *Journal of The Electrochemical Society*, vol. 124, no. 10, p. 1569, 1977.

[71] J. Li, F. Yang, X. Xiao, M. W. Verbrugge, and Y. T. Cheng, "Potentiostatic intermittent titration technique (PITT) for spherical particles with finite interfacial kinetics," *Electrochimica Acta*, vol. 75, pp. 56–61, 2012.

[72] Y. Zhu and C. Wang, "Galvanostatic intermittent titration technique for phase-transformation electrodes," *Journal of Physical Chemistry C*, vol. 2, no. 2, pp. 2830–2841, 2010.

[73] E.Potiron, A. L. G. La Salle, A. Verbaere, Y. Piffard, and D.Guyomard, "Electrochemically synthesized vanadium oxides as lithium insertion hosts," *Electrochemica Acta*, vol. 45, pp. 197–214, 1999.

[74] C. Wang, I. Kakwan, A. J. Appleby, and F. E. Little, "In situ investigation of electrochemical lithium intercalation into graphite powder," *Journal of Electroanalytical Chemistry*, vol. 489, pp. 55–67, 2000.

[75] N. Ding, J. Xu, Y. X. Yao, G. Wegner, X. Fang, C. H. Chen, and I. Lieberwirth, "Determination of the diffusion coefficient of lithium ions in nano-Si," *Solid State Ionics*, vol. 180, pp. 222–225, Mar. 2009.

[76] A. Mukhopadhyay, A. Tokranov, K. Sena, X. Xiao, and B. W. Sheldon, "Thin film graphite electrodes with low stress generation during Li-intercalation," *Carbon*, vol. 49, no. 8, pp. 2742–2749, 2011.

[77] X. Wang, F. Fan, J. Wang, H. Wang, S. Tao, A. Yang, Y. Liu, H. Beng Chew, S. X. Mao, T. Zhu, and S. Xia, "High damage tolerance of electrochemically lithiated silicon," *Nature Communications*, vol. 6, no. 1, p. 8417, Dec. 2015.

[78] S. Rakshit, R. Tripuraneni, and S. P. V Nadimpalli, "Real-time stress measurement in SiO_2 thin films during electrochemical lithiation/delithiation cycling," *Experimental Mechanics*, vol. 58, pp. 537–547, 2018.

[79] C. Chen, E. Chason, and P. R. Guduru, "Measurements of the phase and stress evolution during initial lithiation of Sn electrodes," *Journal of The Electrochemical Society*, vol. 164, no. 4, pp. 574–579, 2017.

[80] M. Pharr, Y. Seok, D. Lee, K. Hwan, and J. J. Vlassak, "Measurements of stress and fracture in germanium electrodes of lithium-ion batteries during electrochemical lithiation and delithiation," *Journal of Power Sources*, vol. 304, pp. 164–169, 2016.

[81] A. Mukhopadhyay and B. W. Sheldon, "Deformation and stress in electrode materials for Li-ion batteries," *Progress in Materials Science*, vol. 63, no. January, pp. 58–116, 2014.

[82] V. A. Sethuraman, V. Srinivasan, A. F. Bower, and P. R. Guduru, "In situ measurements of stress-potential coupling in lithiated silicon," *Journal of The Electrochemical Society*, vol. 157, no. 11, p. A1253, 2010.

[83] M. Z. Bazant, M. S. Kilic, B. D. Storey, and A. Ajdari, "Nonlinear electrokinetics at large voltages," *New Journal of Physics*, vol. 11, no. 75016, pp. 1–9, 2009.

[84] K. T. Chu and M. Z. Bazant, "Nonlinear electrochemical relaxation around conductors," *Physical Review E - Statistical, Nonlinear, and Soft Matter Physics*, vol. 74, no. 1, 2006.

[85] G. Bucci, Y. M. Chiang, and W. C. Carter, "Formulation of the coupled electrochemical-mechanical boundary-value problem, with applications to transport of multiple charged species," *Acta Materialia*, vol. 104, pp. 33–51, 2016.

[86] W. Liang, H. Yang, F. Fan, Y. Liu, X. H. Liu, J. Y. Huang, T. Zhu, and S. Zhang, "Tough germanium nanoparticles under electrochemical cycling," *ACS Nano*, vol. 7, no. 4, pp. 3427–3433, Apr. 2013.

[87] H. Yang, W. Liang, X. Guo, C. M. Wang, and S. Zhang, "Strong kinetics-stress coupling in lithiation of Si and Ge anodes," *Extreme Mechanics Letters*, vol. 2, no. 1, pp. 1–6, 2015.

[88] B. Laforge, L. Levan-Jodin, R. Salot, and A. Billard, "Study of germanium as electrode in thin-film battery," *Journal of The Electrochemical Society*, vol. 155, no. 2, p. A181, 2008.

[89] L. Baggetto and P. H. L. Notten, "Lithium-ion (de)insertion reaction of germanium thin-film electrodes: An electrochemical and in situ XRD study," *Journal of The Electrochemical Society*, vol. 156, no. 3, p. A169, 2009.

[90] M. Gu, H. Yang, D. E. Perea, J. Zhang, S. Zhang, and C. Wang, "Bending-induced symmetry breaking of lithiation in germanium nanowires," *Nano Letters.*, vol. 14, no. 8, pp. 4622–4627, 2014.

[91] X. Wang, A. Yang, and S. Xia, "Fracture toughness characterization of lithiated germanium as an anode material for lithium-ion batteries," *Journal of The Electrochemical Society*, vol. 163, no. 2, pp. A90–A95, 2016.

[92] D. Grazioli, M. Magri, and A. Salvadori, "Computational modeling of Li-ion batteries," *Computational Mechanics*, vol. 58, no. 6, pp. 889–909, 2016.

[93] K. Zhao, M. Pharr, S. Cai, J. J. Vlassak, and Z. Suo, "Large plastic deformation in high-capacity lithium-ion batteries caused by charge and discharge," *Journal of the American Ceramic Society*, vol. 94, no. 1, pp. 226–235, 2011.

[94] C. Masquelier and S. Patoux, "Chemical and electrochemical insertion of lithium into two allotropic varieties of NbPO5Se," *Chemistry of Materials*, vol. 14, pp. 2334–2341, 2002.

[95] J. Hong, C. Wang, and U. Kasavajjula, "Kinetic behavior of LiFeMgPO 4 cathode material for Li-ion batteries," *Journal of Power Sources*, vol. 162, no. August, pp. 1289–1296, 2006.

[96] X. H. Rui, N. Ding, J. Liu, C. Li, and C. H. Chen, "Analysis of the chemical diffusion coefficient of lithium ions in Li3V2(PO4)3 cathode material," *Electrochimica Acta*, vol. 55, no. 7, pp. 2384–2390, 2010.

[97] E. Markevich, M. D. Levi, and D. Aurbach, "Comparison between potentiostatic and galvanostatic intermittent titration techniques for determination of chemical diffusion coefficients in ion-insertion electrodes," *Journal of Electroanalytical Chemistry*, vol. 580, no. 2, pp. 231–237, 2005.

[98] Y. Ho and K. Kanamura, "Li + ion diffusion in Li 4 Ti 5 O 12 thin film electrode prepared by PVP sol – gel method," *Journal of Solid State Chemistry*, vol. 177, pp. 2094–2100, 2004.

[99] G. Bucci, T. Swamy, Y.-M. Chiang, and W. C. Carter, "Modeling of internal mechanical failure of all-solid-state batteries during electrochemical cycling, and implications for battery design," *Journal of Materials Chemistry A*, vol. 5, no. 36, pp. 19422–19430, 2017.

[100] M. W. Verbrugge and B. J. Koch, "Modeling lithium intercalation of single-fiber carbon microelectrodes," *Journal of The Electrochemical Society*, vol. 143, no. 2, p. 600, 1996.

[101] R. Tripuraneni and S. P. V. Nadimpalli, "Real-time measurement of biaxial modulus of Ge anode for Li-ion batteries" *XXIV ICTAM, 21-26 August 2016, Montreal, Canada*, 2016.

[102] M. Papakyriakou, X. Wang, and S. Xia, "Characterization of stress-diffusion coupling in lithiated germanium by nanoindentation," *Experimental Mechanics*, vol. 58, no. 4, pp. 613–625, 2018.

[103] M. J. Aziz, P. C. Sabin, and G. Q. Lu, "The activation strain tensor: Nonhydrostatic stress effects on crystal-growth kinetics," *Physical Review B*, vol. 44, no. 18, pp. 9812–9816, 1991.

[104] H. Haftbaradaran, J. Song, W. A. Curtin, and H. Gao, "Continuum and atomistic models of strongly coupled diffusion, stress, and solute concentration," *Journal of Power Sources*, vol. 196, no. 1, pp. 361–370, 2011.

[105] C. V. Di Leo, E. Rejovitzky, and L. Anand, "International Journal of Solids and Structures Diffusion – deformation theory for amorphous silicon anodes : The role of plastic deformation on electrochemical performance," *International Journal of Solids and Structures*, vol. 67, pp. 283–296, 2015.

[106] R. Purkayastha and R. M. McMeeking, "A Linearized model for lithium ion batteries and maps for their performance and failure," *Journal of Applied Mechanics*, vol. 79, no. 3, p. 31021, 2012.

[107] W. Luo, F. Shen, C. Bommier, H. Zhu, X. Ji, and L. Hu, "Na-ion battery anodes: materials and electrochemistry," *Accounts of Chemical Research*, vol. 49, no. 2, pp. 231–240, 2016.

[108] E. De La Llave, V. Borgel, K. J. Park, J. Y. Hwang, Y. K. Sun, P. Hartmann, F. F. Chesneau, and D. Aurbach, "Comparison between Na-ion and Li-ion cells: understanding the critical role of the cathodes stability and the anodes pretreatment on the cells behavior," *ACS Applied Materials and Interfaces*, vol. 8, no. 3, pp. 1867–1875, 2016.

[109] S. Komaba, W. Murata, T. Ishikawa, N. Yabuuchi, T. Ozeki, T. Nakayama, A. Ogata, K. Gotoh, and K. Fujiwara, "Electrochemical Na insertion and solid electrolyte interphase for hard-carbon electrodes and application to Na-ion batteries," *Advanced Functional Materials*, vol. 21, no. 20, pp. 3859–3867, 2011.

[110] S. W. Kim, D. H. Seo, X. Ma, G. Ceder, and K. Kang, "Electrode materials for rechargeable sodium-ion batteries: Potential alternatives to current lithium-ion batteries," *Advanced Energy Materials*, vol. 2, no. 7, pp. 710–721, 2012.

[111] K. Kubota and S. Komaba, "Review — practical issues and future perspective for Na-ion batteries," *Journal of the Electrochemical Soceity*, vol. 162, no. 14, pp. 2538–2550, 2015.

[112] H. Moriwake, "Why is sodium-intercalated graphite unstable?" *RSC Advances*, vol. 7, pp. 36550–36554, 2017.

[113] P. Thomas, D. Billaud, I. Nancy, and B. P. Vandoeu, "Electrochemical insertion of sodium into hard carbons," *Electrochemcia Acta*, vol. 47, no. 20, pp. 3303–3307, 2002.

[114] C. Bommier and X. Ji, "Recent development on anodes for Na-ion batteries," *Israel Journal of Chemistry*, vol. 55, no. 5, pp. 486–507, 2015.

[115] L. Baggetto, J. K. Keum, J. F. Browning, and G. M. Veith, "Germanium as negative electrode material for sodium-ion batteries," *Electrochemistry Communications*, vol. 34, pp. 41–44, 2013.

[116] S. Komaba, Y. Matsuura, T. Ishikawa, N. Yabuuchi, W. Murata, and S. Kuze, "Electrochemistry communications redox reaction of Sn-polyacrylate electrodes in aprotic Na cell," *Electrochemistry Communications*, vol. 21, pp. 65–68, 2012.

[117] H. Xie, X. Tan, E. J. Luber, B. C. Olsen, W. P. Kalisvaart, K. L. Jungjohann, D. Mitlin, and J. M. Buriak, "β - SnSb for sodium ion battery anodes :phase," *ACS Energy Letters*, vol. 3, pp. 1670–1676, 2018.

[118] L. Baggetto, P. Ganesh, R. P. Meisner, R. R. Unocic, J. C. Jumas, C. A. Bridges, and G. M. Veith, "Characterization of sodium ion electrochemical reaction with tin anodes: Experiment and theory," *Journal of Power Sources*, vol. 234, pp. 48–59, 2013.

[119] J. Wang, F. Fan, Y. Liu, K. L. Jungjohann, S. W. Lee, S. X. Mao, X. Liu, and T. Zhu, "Structural evolution and pulverization of tin nanoparticles during lithiation-delithiation cycling," *Journal of the Electrochemical Society*, vol. 161, no. 11, pp. F3019–F3024, 2014.

[120] R. Kali, Y. Krishnan, and A. Mukhopadhyay, "Effects of phase assemblage and microstructure-type for Sn/intermetallic 'composite' films on stress developments and cyclic stability upon lithiation/delithiation," *Scripta Materialia*, vol. 130, pp. 105–109, 2017.

[121] P. R. Abel, Y. M. Lin, T. De Souza, C. Y. Chou, A. Gupta, J. B. Goodenough, G. S. Hwang, A. Heller, and C. B. Mullins, "Nanocolumnar germanium thin films as a high-rate sodium-ion battery anode material," *Journal of Physical Chemistry C*, vol. 117, no. 37, pp. 18885–18890, 2013.

[122] M. Dahbi, N. Yabuuchi, K. Kubota, K. Tokiwa, and S. Komaba, "Negative electrodes for Na-ion batteries," *Physical Chemistry Chemical Physics*, vol. 16, no. 29, p. 15007, 2014.

[123] S. P. V Nadimpalli, V. A. Sethuraman, G. Bucci, V. Srinivasan, A. F. Bower, P. R. Guduru, E. Technologies, and L. Berkeley, "On plastic deformation and fracture in Si films during electrochemical lithiation/delithiation cycling," *Journal of Electroanalytical Chemistry*, vol. 160, no. 10, pp. 1885–1893, 2013.

[124] R. Tripuraneni, S. Rakshit, and S. P. V Nadimpalli, "In situ measurement of the effect of stress on the chemical diffusion coefficient of Li in high-energy-density electrodes," *Journal of Electroanalytical Chemistry*, vol. 165, no. 10, pp. 2194–2202, 2018.

[125] I. Yoon, D. P. Abraham, B. L. Lucht, A. F. Bower, and P. R. Guduru, "In situ measurement of solid electrolyte interphase evolution on silicon anodes using atomic force microscopy," *Advanced Energy Materials*, vol. 6, no. 12, 2016.

[126] X. Lu, E. R. Adkins, Y. He, L. Zhong, L. Luo, S. X. Mao, C. M. Wang, and B. A. Korgel, "Germanium as a sodium ion battery material: In situ TEM reveals fast sodiation kinetics with high capacity," *Chemistry of Materials*, vol. 28, no. 4, pp. 1236–1242, 2016.

[127] H. Li, J. Y. Huang, S. X. Mao, and T. Zhu, "Two-phase electrochemical lithiation in amorphous silicon" *Nano Letters*, vol. 13, no. 2, pp. 709-715, 2013.

[128] A. Kohandehghan, K. Cui, M. Kupsta, J. Ding, E. Memarzadeh Lotfabad, W. P. Kalisvaart, and D. Mitlin, "Activation with Li enables facile sodium storage in germanium," *Nano Letters*, vol. 14, no. 10, pp. 5873–5882, 2014.